CONF-8310143--54

COMPUTATIONAL METHODS FOR FRACTURE ANALYSIS OF HEAVY-SECTION STEEL TECHNOLOGY (HSST) PRESSURE VESSEL EXPERIMENTS

B. R. Bass†, R. H. Bryan, J. W. Bryson and J. G. Merkle

Oak Ridge National Laboratory*
Union Carbide Corporation, Nuclear Division
Oak Ridge, Tennessee 37830

CONF-8310143--54

DE84 003327

DISCLAIMER

---

* Operated by Union Carbide Corporation under Contract W-7405-eng-26 with with the U. S. Department of Energy.

† Computer Sciences Organization, Union Carbide Corporation, Nuclear Division.

COMPUTATIONAL METHODS FOR FRACTURE ANALYSIS OF HEAVY-SECTION STEEL TECHNOLOGY (HSST) PRESSURE VESSEL EXPERIMENTS*

B. R. Bass†, R. H. Bryan, J. W. Bryson, and J. G. Merkle
Oak Ridge National Laboratory
Oak Ridge, TN 37830

SUMMARY

This paper summarizes the capabilities and applications of the general-purpose and special-purpose computer programs that have been developed at the Oak Ridge National Laboratory (ORNL) for use in fracture mechanics analyses of HSST pressure vessel experiments. Emphasis is placed on the OCA/USA code, which is designed for analysis of pressurized-thermal-shock (PTS) conditions, and on the ORMGEN/ADINA/ORVIRT system which is used for more general analysis. Fundamental features of these programs are discussed, along with applications to pressure vessel experiments.

1. INTRODUCTION

Several general-purpose and special-purpose computer programs have been developed at ORNL for use in analyzing the fracture response of thick-walled pressure vessels tested in conjunction with the HSST program. The programs perform static analyses of brittle or ductile fracture in two-dimensional (2-D) or fully three-dimensional (3-D) geometries. Table 1 summarizes the status and capabilities of each fracture code and indicates the relevant ORNL user documentation for each one. In this paper, the emphasis is placed on capabilities of the OCA/USA program, which is being used for assessments associated with PTS experiments at ORNL, and the ORMGEN/ADINA/ORVIRT system which is used for more general analysis. The ORMGEN/ADINA/ORVIRT system is presented first, followed by applications that include pretest planning and posttest analyses of the ITV V-8A test that was concerned with ductile tearing in a low upper-shelf toughness weldment. This is followed by a discussion of the OCA/USA program and by sample results from applications to the ORNL PTS test configuration.

---

* Research sponsored by the Office of Nuclear Regulatory Research, U. S. Nuclear Regulatory Commission under Interagency Agreements 40-551-75 and 40-552-75 with the U. S. Department of Energy under Contract W-7405-eng-26 with the Union Carbide Corporation.

† Computer Sciences Organization, Union Carbide Corporation, Nuclear Division.

2. THE ORMGEN/ADINA/ORVIRT SYSTEM

2.1 Program Description

The finite element analysis system, ORMGEN/ADINA/ORVIRT, is a three-program system that addresses linear and nonlinear static fracture in 2- and 3-D crack geometries. Program ORMGEN (1)* automatically generates a complete 3-D finite element model of the cracked structure and creates data files which have formats compatible with the ADINA (2) structural analysis program. Special elements that introduce an appropriate stress singularity are used along the crack front. Program ORVIRT (3) acts as a postprocessor of the conventional ADINA analysis. ORVIRT employs a virtual crack extension technique for the calculation of energy release rates at specified points along the crack front.

ORMGEN presently has a library of six 3-D crack geometries which are illustrated in Fig. 1 and are currently of interest to the HSST Program. The library of crack geometries includes flat plates with straight or curved surface cracks and cylinders with part-through cracks on the outer or inner surface. The curved cracks may be semicircular, semielliptical, or user defined. The straight crack in the plate configuration (Fig. 1(b)) is a through-crack, while for a cylinder it is a part-through crack (Fig. 1(d) and Fig. 1(f)). A cladding option is available that allows for either an embedded or a penetrating crack in the clad material. For each of these six crack geometries, ORMGEN provides ADINA-formatted data files that include nodal point coordinates, element connectivities, and appropriate displacements and pressure boundary conditions.

The strategy employed in ORMGEN is to surround the crack front with a core of special crack tip elements (see Fig. 2) and to model the remainder of the structure with conventional 20-node isoparametric brick elements. Element group I of the finite element model consists of the inner core of special crack tip elements enclosed by a single layer of conventional brick elements (Fig. 2). The remaining conventional brick elements of the model constitute element group II.

The special crack tip elements are employed along the crack front to model the appropriate singularity in the stress field. For linear elastic calculations, the quarter-point wedge element of Fig. 3(a) is used at the crack front to allow for a $1/\sqrt{r}$ singularity in the stress and strain fields (4), where r is the radial distance from the crack tip. Figure 3(b) illustrates the collapsed prism element appropriate for a perfectly plastic material, with midside nodes that allow for a 1/r singularity at the crack front (4). In the collapsed element, the nodes that initially share the same locations at the tip will separate with increasing load to allow for

---

* Numbers in parentheses refer to the references given at the end of this paper.

blunting of the crack (see Fig. 4). The program allows the user to select either of the two special crack tip elements, depending upon whether the application is for linear elastic fracture analysis or for ductile fracture analysis.

The ORVIRT fracture mechanics program utilizes a virtual-crack-extension technique developed by deLorenzi (5) for isothermal applications and modified by Bass and Bryson (6) to account for thermal strains in cracked bodies. The technique requires calculation of the released energy G* corresponding to a small crack advance in a cracked body subjected to surface tractions F_α, body force f_α, and temperature distribution T (see Fig. 5). Points of configuration I (prior to crack advance) are mapped into configuration II (after crack advance) by the mapping

$$\bar{x}_\alpha = x_\alpha + \Delta x_\alpha(x_\beta) \tag{1}$$

where x_α, $\bar{x}_\alpha$ correspond to coordinates in configurations I and II, respectively, and Δx_α is the incremental change in coordinates. From Refs. 5 and 6, the total energy release rate G_T is given by

$$G_T = G^*/\Delta A \tag{2}$$

where ΔA is the area increment covered by the virtual extension of the crack front (see Fig. 6), and

$$G^* = \int_V \left(\sigma_{\alpha\beta} \frac{\partial u_\alpha}{\partial x_\delta} - W\delta_{\delta\beta} \right) \frac{\partial \Delta x_\delta}{\partial x_\beta} \, dV + \int_V \left(\sigma_{\alpha\beta} \frac{\partial \theta_{\alpha\beta}}{\partial x_\delta} - f_\alpha \frac{\partial u_\alpha}{\partial x_\delta} \right) \Delta x_\delta dV \tag{3}$$

In Eq. (3), $\sigma_{\alpha\beta}$ are the components of the stress tensor, u_α are displacement components, $\theta_{\alpha\beta}$ are the strains of free thermal expansion, x_δ are spatial coordinates, and dV is the volume differential. The strain energy density W is given by

$$W = \int_o^{\varepsilon'_{\gamma\delta}} \sigma_{\alpha\beta} d\varepsilon'_{\alpha\beta} \, , \quad \varepsilon'_{\alpha\beta} = \varepsilon_{\alpha\beta} - \theta_{\alpha\beta} \tag{4}$$

where the mechanical strain components $\varepsilon'_{\alpha\beta}$ are defined in terms of the total strains $\varepsilon_{\alpha\beta}$ and the thermal strains $\theta_{\alpha\beta}$. Average and local values of G_T are evaluated, respectively, from uniform and local virtual extensions of the crack front (see Fig. 6).

In applications, the energy release rate G_T of Eqs. (2), (3) is evaluated numerically from solution data written to the nodal point and element portholes of ADINA and from a user-supplied virtual extension Δx_α of the crack front. The ORMGEN mesh generator program interfaces with the ORVIRT program to perform this integration in a particularly efficient manner. When applied to an ORMGEN-generated finite element model, program ORVIRT evaluates the volume integral of Eq. (3) only over the crack front element group I (Fig. 2), using a virtual crack extension file created automatically by ORMGEN.

2.2 Applications to the V-8A Pressure Vessel Test

The ORMGEN/ADINA/ORVIRT system has been applied to pretest planning and to posttest analyses of the ITV V-8A test (7) conducted by the HSST program. The objective of the test was to provide accurate quantitative data concerning the growth of ductile tearing and final instability of a crack in a low upper-shelf toughness weldment located in a cylinder of reactor vessel steel. The motivation for performing this test is that there are vessels in service containing welds which, because of high copper content, may have their Charpy upper-shelf energy values reduced to relatively low levels by neutron irradiation. After some period of operation, the toughness of these welds is expected to be degraded to the extent that practical operating temperature limits may not be attainable in accordance with present regulatory guidelines. The results of the V-8A test are intended to provide an experimental basis for judging the accuracy of vessel fracture safety analysis procedures for low upper-shelf toughness conditions.

The purposes for which the V-8A test plan was formulated are (1) to demonstrate the fracture behavior of low-toughness material at upper-shelf temperatures and (2) to provide a basis for comparisons between elastic-plastic fracture-mechanics predictions of stable and unstable tearing and full-scale test results. Accordingly, the plan involved the placement of a large crack in a special low upper-shelf weld seam that was in turn placed in a test vessel as shown in Fig. 7. A crack having an approximate semielliptical profile 280 mm long by 70 mm deep was machined in the seam and fatigue-cycled to a depth of 88 mm. Pretest ultrasonic measurement indicated that the initial crack was 91 mm deep. Then, with the vessel heated to the proper temperature, the vessel was pressurized slowly with intermittent pauses for recording data related to crack growth until unstable tearing was detected. After an instability was observed, the vessel was depressurized to preserve the crack and the vessel for further examination.

For the final pretest predictions of crack behavior, three-dimensional finite element analyses were performed with ORMGEN/ADINA/ORVIRT for a range of crack depths and internal pressures using a material model that is based on the deformation theory of plasticity (8). Energy release rates computed from these analyses were compared with available tearing resistance data to estimate the onset of stable tearing as well as unstable tearing of the crack. Figures 8 and 9 show the dimensions of a quarter section of the

test vessel as modeled and a portion of the finite element discretization generated by ORMGEN. The experimental material response (uniaxial stress-strain curve) was modeled using a multilinear approximation as depicted in Fig. 10. For the models that were analyzed, values of material properties were taken to be: Young's modulus $E = 0.2095 \times 10^6$ MPa, Poisson's ratio $\nu = 0.3$, and initial yield stress $\sigma_y = 427.5$ MPa.

Results from the analysis of one of these cases, V8EP9 (a = 98 mm, b = 140 mm), are presented in Fig. 11 in terms of $J_I(\phi,p)$, where $J_I = G_I$ is evaluated from Eq. (2); pressure p is a parameter. The J_I values peak sharply around $\phi = 20^\circ$ to 30° at the higher pressures (140-155 MPa), in contrast to the J_I distribution for pressures producing no large-scale yielding (105 MPa). The computed J_I values were used in conjunction with measured tearing resistance curves (9) (Fig. 12) to make estimates of J_R-controlled tearing. The scheme for determining the progression of J_R-controlled tearing is illustrated in Fig. 13. If a crack has an initial depth a_o, then at some pressure, p_1, the condition $J_I = J_R$ is satisfied when $a = a_1$ and $J_I = J_{R1}$. In this particular instance, as shown in Fig. 13, at a constant pressure, p_1, a virtual increment in crack depth beyond a_1 would cause J_R to increase more than J_I with the result that $J_R > J_I$. This implies that more energy would be required to generate the virtual extension than could be supplied by the strain energy released; thus, a_1 is a stable crack depth. At crack depths a_2 and a_3, a virtual extension would result in $J_I > J_R$ and a tearing instability. Pressure p_2 is the maximum pressure determined by this procedure for which $J_I = J_R$ and is therefore defined as the tearing instability pressure.

Two independent ORNL predictions of conditions for tearing instability were made on the basis of the J_R curves of Fig. 12 and results from applications of ORMGEN/ADINA/ORVIRT to a series of crack models (7). These predictions, along with those made by other groups, are shown in Table 2. The diverseness of the resistance curves accounts for the differences in ORNL predictions of the instability pressure. The ORNL predictions for stable crack growth were not very sensitive to the choice of a J_R curve. All of the estimated instability pressures are within the range of 87 to 110% of the measured instability pressure of ~ 139 MPa. The predicted estimates of crack growth prior to instability range from 6.8 to 15 mm.

After the V-8A test, the segment of the weld containing the crack was cut from the vessel and split to expose the crack surface. Figure 14 shows clearly the initial machined and fatigue-sharpened profiles as well as the final canoe-shaped profile attained in the test. Measurements of initial and final crack dimensions indicate that the pretest values given in Table 3 were reasonably accurate. Results of the J_R specimen test (10) for the weld material are given in Fig. 12 and show that the V-8A weld seam had a relatively low tearing resistance when compared to characterization weld data.

Additional fracture analyses of the V-8A test are being performed on the basis of these posttest measurements of geometry and properties. Figure 15 illustrates a series of four crack profiles, where profile 1 is the initial configuration and profile 4 the final configuration, that were analyzed with the ORMGEN/ADINA/ORVIRT system. The ORMGEN-generated finite element model of profile 4 is depicted in Fig. 16. Results from these four analyses are presented in Figs. 17-21 for $J_I(\phi,p)$ and in Fig. 22 for crack mouth opening displacement (CMOD). These analyses indicate that the peak values of J_I associated with the initial profile 1 for $\phi \approx 20^o$ and $p \geq 135$ MPa are reduced relative to the maximum depth values at $\phi = 90^o$ as the crack profile progressively takes on the canoe-like shape of the final configuration. This is illustrated by the family of $J_I(\phi,p)$ curves shown in Fig. 21 for the progression of four crack profiles at a single pressure, 135 MPa (near which most of the tearing occurred in the test). Profile 1 (semi-ellipse) shows a relatively high driving force for crack extension in the directions of $10^o \leq \phi \leq 20^o$; progressive canoeing (profiles 2-4) appears to diminish this tendency. These analytical results are in agreement qualitatively with the experimental observations that little, if any, axial crack growth occurred at pressures below ~ 138 MPa, while extensive canoeing occurred at or above this pressure.

Further analyses are currently under way that combine the above results for J_I values with updated J_R data to make posttest computational estimates of conditions for tearing instability. The comparisons between measured and computed CMOD values in Fig. 22 reflect that the stress-strain curve of Fig. 6 used to model the vessel material is overly stiff in the elastic region. An adjusted stress-strain curve that reflects the posttest measured properties will be employed in a repetition of the above analyses.

3. THE OCA/USA PROGRAM

3.1 Program Description

Extensive computational analyses are being performed to determine material parameters and optimum pressure-temperature transients compatible with proposed pressurized-thermal-shock (PTS) test (11) scenarios and with the capabilities of the PTS test facility (Fig. 23) at ORNL. Both linear and nonlinear material models are employed, as well as 2-D and 3-D finite element representations of crack geometries. Computational economy requires application of techniques suitable for parametric studies involving a large number of transients. These techniques, which include the use of a 3-D superposition method, an inelastic ligament stability assessment, and an upper-shelf arrest analysis, have been incorporated into the previously developed OCA-I (12) code to form the OCA/USA computer program.

Basic calculations performed by OCA/USA are (1) a thermal analysis to provide the temperature history through the vessel wall; (2) a stress analysis that provides the circumferential stresses for the uncracked cylinder for combined pressure-thermal loading; (3) computations of initiation factors K_{Ic} and arrest factors K_{Ia} as functions of crack depth and time from material property data and temperature history; (4) 2-D and 3-D superposition analyses that provide the stress intensity factors K_I as a function crack depth and time; (5) an interpolation of the computed factors K_I, the initiation factors K_{Ic}, and the arrest factors K_{Ia} to determine the times for each crack depth at which $K_I = K_{Ic}$, $K_I = K_{Ia}$, and $dK_I/dt = 0$; (6) a ligament stability analysis based on an ideally-plastic material model; (7) an upper-shelf arrest analysis based on tearing resistance (J_R) criteria; (8) extensive postprocessing graphics output. Items (1), (2), (3), (4) (for 2-D superposition), (5), and (8) above have been described in Ref. (12) and the remaining items (4) (for 3-D superposition), (6), and (7) are presented here.

The surface crack shown in Fig. 23 was analyzed initially by assuming an infinitely long (2-D) crack and using superposition techniques to calculate K_I factors for time-dependent combined pressure and thermal loading. To obtain improved estimates for K_I values, direct 3-D calculations (13) were performed with ORMGEN/ADINA/ORVIRT for a range of depth ratios; the crack was postulated to grow deeper without increasing in length. To avoid the prohibitively high computing cost of the direct 3-D approach for time-varying boundary conditions, an alternative superposition technique (14,15) was adopted. Considerable economy can be achieved in this approach since the only 3-D solutions required are those used to calculate a set of influence coefficients for a given crack model. In Fig. 24, these influence coefficients are stress intensity factors ${}^jK_I(\phi)$, $j = 0, 1, 2, 3$, computed from crack surface loading functions ${}^j\sigma(y) = (y/a)^j$. To obtain the $K_I(\phi)$ distribution for an arbitrary loading condition, the hoop stress distribution $\sigma(y)$ from an uncracked cylinder is expressed as a third-order polynomial

$$\sigma(y) = \sum_{j=0}^{3} c_j (y/a)^j \quad . \tag{5}$$

Then, by superposition, the K_I function is calculated from the influence coefficients ${}^jK_I$ and the coefficients of Eq. (5) according to

$$K_I(\phi) = \sum_{j=0}^{3} c_j \, {}^jK_I(\phi) \quad . \tag{6}$$

For the crack geometry of Fig. 23, the influence coefficients ${}^{j}K_{I}$ (ϕ) were calculated for a set of depth ratios a/w = {.1,.2,.3,.4,.5,.6,.9} using the ORMGEN/ADINA/ORVIRT system. The 3-D superposition technique is compared in Fig. 25 with direct 3-D thermoelastic analyses from ORMGEN/ADINA/ORVIRT with the parameters of the PTS transient T1 given in Table 4. Results are presented for surface cracks of depth a/w = 0.1 and 0.6. Also shown in the figure are results for infinitely long cracks of the same a/w ratios. The latter results illustrate the difference between infinite crack and finite crack models for the deeper cracks in this series.

Another consideration in the PTS transient is that the upper shelf be reached at a crack depth/pressure combination that precludes tensile instability of the remaining ligament. At the unstable crack depth corresponding to the ligament fully yielded in tension, stretching of the ligament causes large increases in crack tip opening displacement. The model implemented in OCA/USA for this condition assumes a deep continuous surface crack with complete ligament yielding, but without strain-hardening (16). Because the crack is deep, a strip-yield type model was adopted such that yielding occurs only on the plane ahead of the tip. Thus, when the ligament is completely yielded, the stress distribution directly ahead of the crack is ideally plastic (Fig. 26).

In Ref. 16, a section of the cylinder (subjected to radially symmetric loading) is modeled as a cut ring (Fig. 26) with one face clamped and the other free. The crack face tractions are derived for the model and used to determine the crack face rotation θ and the ratio d/b. The latter ratio locates the hinge point or the point of stress reversal in the fully yielded remaining ligament. For the hinge point located inside the remaining ligament, d/b > 0, the crack tip opening displacement δ is given by

$$\delta = \theta w \left(\frac{b}{w}\right)\left(1 - \frac{d}{b}\right) \quad . \tag{7}$$

For the ligament fully yielded in tension and the hinge point located outside the ligament, the stress distribution in the ligament is independent of the hinge point location, being the same as for d = 0. The tip displacement for this case is given by

$$\delta = -\Delta y - \theta w \left(\frac{1}{2} - \frac{b}{w}\right) \quad . \tag{8}$$

The foregoing model, implemented in the OCA/USA code, is compared with two other analyses in Fig. 27 for the PTS transient T1 of Table 4. The figure shows results from the ideally-plastic ligament model at 6 min in the transient T1 in the form of a pseudo K_J-value obtained from the relations $K_J = \sqrt{EJ}$, $J = \sigma_y \delta$, and Eq. (7) or (8). At a/w = 0.69, the ligament becomes completely yielded in tension, causing large increases in crack tip opening displacement. Ligament yielding causes K_J to significantly exceed the linear elastic K_I value prior to development of complete tensile yielding in the remaining ligament. The lower intersection of the two curves identifies the crack depth below which the ideally-plastic analysis should be disregarded because the remaining ligament is not yet completely yielded. To evaluate the reliability of the yielded ligament model, direct thermo-elastic-plastic analyses were performed for a series of crack depths. These studies utilized 2-D plane strain finite element models, a deformation plasticity material model with initial thermal strains (8), a multilinear strain hardening curve having parameters described in Ref. 17 and the ORMGEN/ADINA/ORVIRT system. As expected, the latter analyses considering strain-hardening produced pseudo K_J-values lying between the linear curve and the ideally-plastic curves of Fig. 27. These results emphasize the need to consider plastic instability in PTS analyses for deeper cracks.

An additional enhancement of OCA/USA was motivated by a proposed PTS test scenario in which the crack initiates in cleavage and propagates into a region where temperatures are sufficiently high for completely ductile fracture. An upper-shelf fracture model was developed which assumes the existence of a temperature T_D, above which ductile fracture (even though fast) prevails, and below which fracture is entirely by the cleavage mode. Transitional behavior involving simultaneous cleavage and ductile fracture during a small increment of cracks growth is ignored.

In PTS transients of practical interest, a growing crack runs into a monotonically increasing temperature field, with the ductile upper-shelf regime having $T > T_D$. Dynamic tests of large specimens indicate that T_D is in the neighborhood of ~ 100K higher than the reference nil-ductility temperature RT_{NDT}; at such temperatures crack arrest toughness data are generally unavailable. Under these circumstances, the extrapolated K_{Ia} curve from Section XI (Appendix A) of the ASME code does not appear to be the most reliable basis for planning upper-shelf arrest experiments. As an alternative, the model presented here utilized available tearing resistance (J_R) data to determine whether a crack in the region $T > T_D$ is stable in a quasi-static sense.

The procedure for determining upper-shelf stability is illustrated in Fig. 28. Temperatures in the wall of the vessel during a transient can be represented as contours in a crack depth vs time (a vs t) plot, Fig. 28(a). At a given time t', there is a crack depth a' at which temperature $T = T_D$. It is postulated that the continued growth of the crack with depth a' is controlled by J_R, which is generally a function of incremental crack growth $\Delta a = a - a'$ and crack tip temperature. As illustrated in Fig. 28(b)

for $t = t'$, the condition for crack growth is

$$J_I(a) > J_R[a - a', T(a)] \tag{9}$$

and for stability,

$$J_I(a) \leq J_R[a - a', T(a)] \quad . \tag{10}$$

Application of the technique involves a plastic zone size correction to previously calculated K_I values, conversion of K_I to J_I, and computation of stable and unstable upper-shelf points based on the criteria given by Eqs. (9)-(10). The point of incipient instability is defined as the last stable J_R-controlled crack depth.

3.2 Application to Critical-Crack-Depth Analysis

The objectives of the first PTS test to be performed at ORNL (PTSE-1) are to obtain (in chronological order):

1. first initiation in cleavage of a shallow crack prior to first warm prestress (18) WPS1,
2. first arrest in the transition region,
3. $K_I/K_{Ic} \geq 1$ before the end of WPS1,
4. frangible second initiation after WPS1 is relieved, and
5. ductile upper-shelf arrest of a fast-moving crack.

This section describes results from a critical-crack-depth analysis performed with the OCA/USA program using parameters of PTS trial transient T2 in Table 4. The tearing resistance data are characterized by a power law curve, also given in Table 4. The computed factors K_I, the initiation factors K_{Ic} and the arrest factors K_{Ia} are interpolated by the program for a series of crack depths ($0 \leq a/w \leq 0.9$) to determine the times in the transient at which $K_I = K_{Ic}$, $K_I = K_{Ia}$, and $dK_I/dt = 0$. This information is output in the form of critical-crack-depth curves that indicate behavior of the crack during portions of the transient. The curves for transient T2 are presented following a discussion of the criteria used to establish optimum test parameters.

Test parameters are selected to satisfy the criteria summarized in Fig. 29 for a representative K_I vs time transient. These criteria are necessary to account for experimental uncertainties and to provide conclusive evidence of the fracture mechanisms being studied. The first two criteria ensure that the ratio K_I/K_{Ic} is sufficient to guarantee initiation prior to WPS1. The third criterion ensures that K_I is greater than K_{Ic} when WPS1 is removed; in this event there would be no ambiguity about the cause of reinitiation. The fourth criterion ensures that, before the onset of WPS2, the post-WPS1 value of K_I will exceed the maximum value initially obtained; this allows for the possibility that initiation after

WPS1 requires a higher K_I value. The fifth criterion establishes a negative dK_I/dt during WPS1. The sixth criterion ensures a frangible second initiation. The seventh and eighth criteria imply that cleavage arrest would not intervene in the interval $t_5 < t < t_6$ and that arrest would occur on the ductile upper shelf without ligament instability.

Figure 30 shows the critical-crack-depth and K_I vs time plots generated by OCA/USA for transient T2 of Table 4. The curves are constructed by the program from the larger K_I value calculated at each crack depth in two 2-D analyses: the ideally-plastic ligament analysis and the superposition analysis with plastic zone size correction. For (a/w) = 0.05, the first initiation and arrest event can occur in the time interval 0.95 min $\leq t \leq$ 2.0 min, with arrest in the interval $0.11 \leq (a/w)_2 \leq 0.20$. The first WPS starts 2 min into the transient and lasts until the pressure ramp is initiated 4 min later. The crack again becomes critical ($K_I/K_{Ic} \geq 1$) before the end of WPS1, with the second initiation taking place between 6 and 8 min. Initiation is frangible and, if prior to 7.3 min, the arrest will be on the upper shelf in the interval $0.50 \leq (a/w)_{USA} \leq 0.77$; a crack initiating after 7.3 min will not arrest. The ideally-plastic ligament instability curve, also given in Fig. 30, indicates that a plastic instability would not interfere with stable tearing of the crack for the second initiation occurring earlier than 7.3 min. The results presented in Fig. 30 demonstrate that, by restricting $t_6 < 7.3$ min, transient T2 satisfies all but criteria 4 and 7 listed in Fig. 29 when analyzed by a 2-D model. Further evaluation of the transient requires that the critical-crack-depth analysis be repeated using max $K_{I(3-D)}$ values obtained from the 3-D superposition technique and subjected to plastic zone size correction (not shown due to space limitations). Final selection of PTS test parameters will be influenced by additional analyses that examine the sensitivity of the criteria to variation in material properties and test conditions and by fully 3-D thermo-elastic-plastic analyses.

ACKNOWLEDGMENT

This work was supported by the U. S. Nuclear Regulatory Commission through the Heavy-Section Steel Technology program at the Oak Ridge National Laboratory, Oak Ridge, Tennessee. The Oak Ridge National Laboratory is operated by Union Carbide Corporation, Nuclear Division, for the U. S. Department of Energy under U. S. government contract W-7405 eng 26.

REFERENCES

1. BASS, B. R. and BRYSON, J. W.
Applications of Energy Release Rate Technique to Part-Through Cracks in Plates and Cylinders, Volume 1. ORMGEN-3D: A Finite Element Mesh Generator for 3-Dimensional Crack Geometries, NUREG/CR-2997, Vol. 1 (ORNL/TM-8527/V1), Oak Ridge National Laboratory, Oak Ridge, Tenn., December 1982.

2. BATHE, K. J.
"ADINA - A Finite Element Program for Automatic Dynamic Incremental Nonlinear Analysis"
Report 82448-1, Massachusetts Institute of Technology, Cambridge, Mass., September 1975 (revised December 1978).

3. BASS, B. R. and BRYSON, J. W.
Applications of Energy Release Rate Techniques to Part-Through Cracks in Plates and Cylinders, Volume 2. ORVIRT: A Finite Element Program for Energy Release Rate Calculations for 2-D and 3-D Crack Models, NUREG/CR-2997, Vol. 2 (ORNL/TM-8527/V2), Oak Ridge National Laboratory, Oak Ridge, Tenn., February 1983.

4. BARSOUM, R. S.
"Triangular Quarter-Point Elements as Elastic and Perfectly-Plastic Crack Tip Elements"
International Journal for Numerical Methods in Engineering, Vol. 11, 1977, pp. 85-98.

5. DeLORENZI, H. G.
"On the Energy Release Rate and the J-Integral for 3-D Crack Configurations"
TIS Report 80CRD113, General Electric Company, Schenectady, N. Y., June 1980.

6. BASS, B. R. and BRYSON, J. W.
"Energy Release Rate Techniques for Combined Thermo-Mechanical Loading"
Int. Journ. of Fracture, Vol. 22, p. R3, 1983.

7. BRYAN, R. H., et al.
"Experimental Investigation of Tearing Behavior of a Flaw in a Thick Pressure Vessel"
SMiRT Post Conference Seminar No. 6, Monterey, Calif., August 29-30, 1983.

8. BASS, B. R., et al.
"Deformation Theory of Plasticity with Initial Thermal Strains"
In: Heavy-Section Steel Technology Program Quarterly Progress Report for January-March 1983, NUREG/CR-3334, Vol. 1 (ORNL/TM-8787/VI), Oak Ridge National Laboratory, Oak Ridge, Tenn., p. 3, September 1983.

9. DOMAIN, H. A.
"Vessel V-8 Repair and Preparation of Low Upper-Shelf Weldment"
Final Report, Contracts CRD-1055, CRD-1078, The Babcock and Wilcox Company, Alliance, Ohio, January 1982.

10. DOMAIN, H. A. and FUTATO, R. J.
"J-Integral Test Results of HSST-ITV8A Low Upper Shelf Weld"
The Babcock and Wilcox Company, Alliance, Ohio, submitted to Union Carbide Corporation, Nuclear Division, 1983.

11. BRYAN, R. H. and McCULLOCH, R. W.
"Pressurized-Thermal-Shock Studies," In: Heavy-Section Steel Technology Program Quarterly Progress Report for October-December 1982, NUREG/CR-2751, Vol. 4, (ORNL/TM-8369/V4), Oak Ridge National Laboratory, Oak Ridge, Tenn., p. 79, May 1983.

12. ISKANDER, S. K., CHEVERTON, R. D., and BALL, D. G.
OCA-I, A Code for Calculating the Behavior of Flaws on the Inner Surface of a Pressure Vessel
ORNL/NUREG-84, Oak Ridge National Laboratory, Oak Ridge, Tenn., August 1981.

13. BRYSON, J. W. and McCULLOCH, R. W.
"Comparisons of 3-D and 2-D Computed K-Values for Outside Surface Flaws in an ITV for Combined Pressure-Thermal Loading" In: Heavy-Section Steel Technology Program Quarterly Progress Report for October-December 1982) NUREG/CR-2751, Vol. 4 (ORNL/TM-8369/V4), Oak Ridge National Laboratory, Oak Ridge, Tenn., p. 87, May 1983.

14. HELIOT, J., LABBENS, R. C., and PELLISSIER-TANON, A.
"Semi-Elliptical Cracks in a Cylinder Subjected to Stress Gradients," In: Fracture Mechanics, ASTM STP677 (Ed. C. W. Smith), p. 341, 1979.

15. RAJU, I. S. and NEWMAN, J. C.
"Stress Intensity Factor Influence Coefficients for Internal and External Surface Cracks in Cylindrical Vessels," In: Aspects of Fracture Mechanics in Pressure Vessels and Piping, ASME Pub. PVP Vol. 58, p. 37, 1982.

16. MERKLE, J. G.
"Elastic-Ideally-Plastic PTS Analysis for a Deep Continuous External Longitudinal Crack in a Cylinder," In: Heavy-Section Steel Technology Program Quarterly Progress Report for January-March 1983, NUREG/CR-3334, Vol. 1 (ORNL/TM-8787/VI), Oak Ridge National Laboratory, Oak Ridge, Tenn., p. 103, September 1983.

17. BASS, B. R., et al
"Applications of Energy Rate Techniques to Part-Through Cracks in Experimental Pressure Vessels"
ASME Journal of Pressure Vessel Technology, Vol. 104, p. 308, 1982.

18. LOSS, F. J., GRAY, R. A., and HAWTHORNE, J. R.
"Significance of Warm Prestress to Crack Initiation During Thermal Shock," Report NRL/NUREG-8165, Naval Research Laboratory, NTIS, September 1977.

Fig. 1. Six crack configurations automatically generated by ORMGEN

Fig. 2. Crack tip region generated by ORMGEN

Fig. 3. Special crack tip elements employed by ORMGEN

Fig. 4. Collapsed prism elements appropriate for nonlinear analysis

Fig. 5. Crack configuration before and after crack extension

Fig. 6. Virtual crack extension for calculating energy release rate G_T for (a) uniform and (b) local extension

Fig. 7. Schematic view of vessel V-8A

Fig. 8. Description of ITV V-8A cylinder analyzed showing crack and quarter cylinder as modeled.

Fig. 9. Detail of finite element model of intermediate test vessel

Fig. 10. Uniaxial stress-strain curve for intermediate test vessel V-8A material

Fig. 11. J_I vs ϕ and p for case V8EP9 (a = 98 mm, b = 140 mm)

Fig. 12. A comparison of power-law J_R curve fit to characterization weld data and J_R data for the V-8A special seam weld

Fig. 13. Schematic for determination of J_R-controlled crack depth and tearing instability pressure of a vessel

Fig. 14. Fracture surface (side B) developed during V-8A test. The ductile fracture surface is the relatively dark contiguous area bounded by the fatigue crack extension and the light-tone brittle fracture regions generated during posttest fracturing at ~ -196° C.

Fig. 26. Ideally-plastic ligament model in an externally cracked cylinder

Fig. 27. Comparison of ligament analyses for PTS transient T1 of Table 4 at t = 6 min

Fig. 28. Upper-shelf arrest analysis based on J_R-controlled tearing

Fig. 29. Test conditions and criteria for optimization of PTS test parameters

Fig. 30. Critical crack depth and K_I vs time for PTS transient T2 of Table 4. Numbers in circles refer to criterion numbers of Fig. 29

Table 1 Summary of HSST computer programs for fracture analysis

ORNL Developed Fracture Codes

Fracture Code	Date Developed	Numerical Method	Geometry	Nonlinear Material Behavior	Comments
OCA/USA	Under Development	Influence Function	2-D, Limited 3-D	Limited	An enhanced version of OCA-II, designed primarily for pressurized-thermal shock experiments
OCA-P	June, 1983 (Report to be published)	Influence Function, Monte Carlo	2-D, Limited 3-D	No	Probabilistic fracture code employing a Monte Carlo simulation technique
OCA-II	May, 1983 (Report in preparation)	Influence Function	2-D, Limited 3-D	No	Outstanding post-processing capabilities, especially sutiable for parametric analyses of surface flaws in PWR and ITV geometries
ORVIRT	Feb., 1983 NUREG/CR-2997 Vol. 2 ORNL/TM-8527/V2	Finite Element (Virtual Crack Extenstion)	2-D, 3-D	Yes	Versatile and powerful fracture code, interfaces with ORMGEN and ADINA
ORMGEN	Dec., 1982 NUREG/CR-2997 Vol. 1 ORNL/TM-8527/V1	Finite Element Mesh Generator	3-D	N/A	Generates a 3-D finite element model for cracked plates or cylinders in an ADINA compatible format
ORFLAW	April, 1982 NUREG/CR-2494 ORNL/CSD/TM-165	Finite Element (Embedded K)	3-D	No	Developed under subcontract to S. Atluri, Georgia Tech, 3-D, linear elastic only, automatic mesh generation.
OCA-I	August, 1981 NUREG/CR-2113 ORNL/NUREG-84	Influence Function	2-D	No	Strictly 2-D analysis of surface flaws in PWR and ITV geometries
NOZFLAW	March, 1981 NUREG/CR-1843 ORNL/NUREG/CSD/TM-18	Finite Element (Embedded K)	3-D	No	Developed under subcontract to S. Atluri, Georgia Tech. Addresses nozzle corner flaws only, automatic mesh generation.
FMECH	Feb., 1981 NUREG/CR-1499 ORNL/NUREG/CSD/TM-14	Finite Element (Virtual Crack Extension)	2-D	No	First ORNL developed code, limited capabilities relative to more recently developed codes.

Outside Codes that Interface with ORNL Computer Programs

Fracture Code	Date Developed	Numerical Method	Geometry	Nonlinear Material Behavior	Comments
BIGIF	1978 EPRI RP-700-1	Influence Function	2-D, Limited 3-D	No	Developed under EPRI sponsorship, widely used by utilities
ADINA	1975 (rev. 1978) MIT Report 92448-1	Finite Element	2-D, 3-D	Yes	A general purpose finite element code for structural analysis developed by K. J. Bathe at MIT

Table 2. Vessel V-8A pretest predictions for ductile crack instability

	Organization	Method	Pressure (MPa)	Pressure (psi)	Outside Circumferential Strain %	a (mm)	a (in.)
1.	Nat. Bureau of Stds., Boulder, CO	Simplified Line Spring	153	22,200	0.126	11.9	0.47
2.	ORNL - A	Tangent Modulus	150	21,700	0.133	10.2	0.40
3.	IWM, Freiburg	(not specified)	147.4	21,379		15.0	0.59
4.	ORNL - B	ORVIRT	147	21,321		10.0	0.39
5.	CERL (UK)	RG	141	20,450		7.0	0.28
6.	ORNL - C	ORVIRT	139	20,160		8.0	0.31
7.	AERE (UK)	RG	128	18,560		7.0	0.28
8.	Nat. Nuclear (UK)	RG	121	17,550	0.092	6.8	0.27

Table 3. Crack geometry measurements

Measurement	Dimensions (mm)	
	Pretest	Posttest
Wall thickness (w) at flawed section		
Initial	144.5	144.5
Final		139.0
Flaw depth (a)		
Initial	91.2	88.0
Final		102.5
Flaw length (2b)		
Initial	280.0	280.0
Final		456.0

Table 4. PTS parameters for transients T1 and T2 used in the present study

Constants

PTS transient no.	Initial temperature T_o(°C)	RT_{NDT}(°C)	T_D(°C)	Heat transfer coefficient h($wm^{-2}k^{-1}$)
T1	191	13	120, 130	5675
T2	290	52	170	5675

Variables (linear between time points)

Time (min)	Coolant temperature (°C) T1	T2	Pressure (MPa) T1	T2
0	-23	5	27.6	0.5
1	.	.	.	0.5
2	.	.	.	15
3	.	.	27.6	.
4	.	.	20.7	.
5	.	.	48.3	.
6	.	.	82.7	10
8	.	.	.	50
20	12	15	82.7	50

ORNL-DWG 82-16086A

ornl

SIX CRACK CONFIGURATIONS AUTOMATICALLY GENERATED BY ORMGEN

PLATE

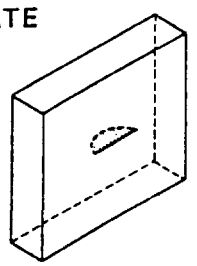

(a) CURVED

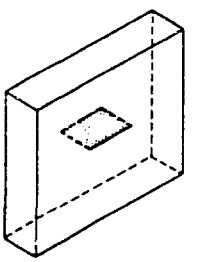

(b) STRAIGHT EDGE

CYLINDER

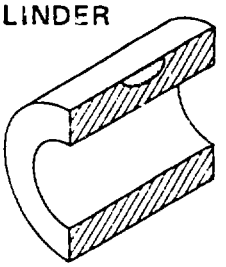

(c) CURVED CRACK ON OUTSIDE SURFACE

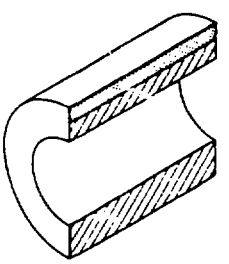

(d) STRAIGHT EDGE CRACK ON OUTSIDE SURFACE

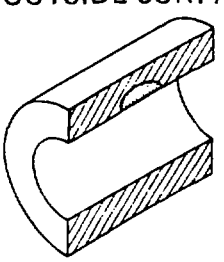

(e) CURVED CRACK ON INSIDE SURFACE

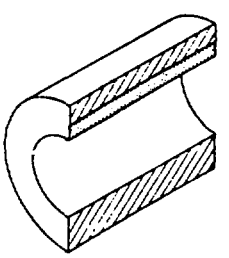

(f) STRAIGHT EDGE CRACK ON INSIDE SURFACE

FIG. 1

ORNL–DWG 82–16085A

ornl

CRACK TIP REGION GENERATED BY ORMGEN

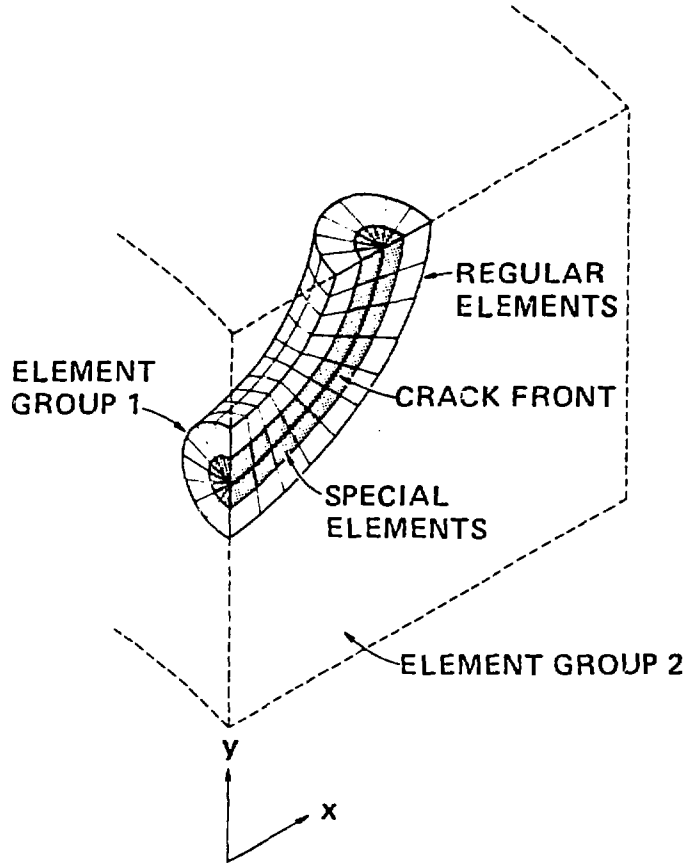

FIG. 2

ORNL–DWG 82–16084A

ornl

SPECIAL CRACK TIP ELEMENTS EMPLOYED IN ORMGEN

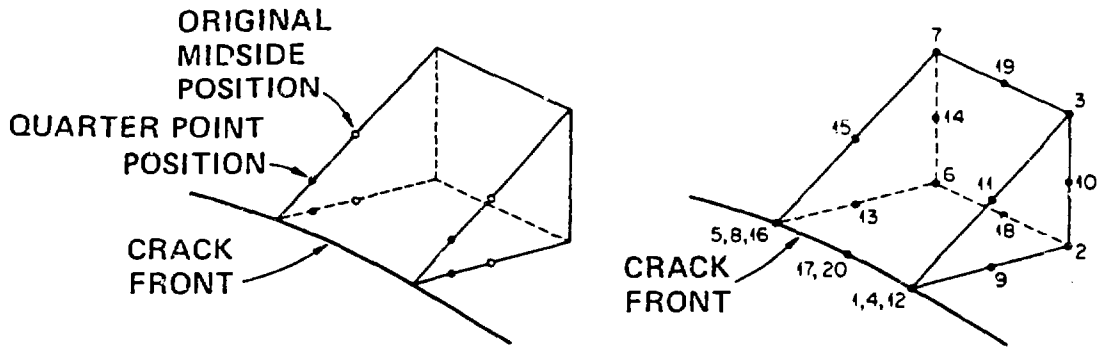

(a) DISTORTED WEDGE ELEMENT

(b) 20–NODE WEDGE ELEMENT

FIG. 3

ORNL-DWG 82-16083

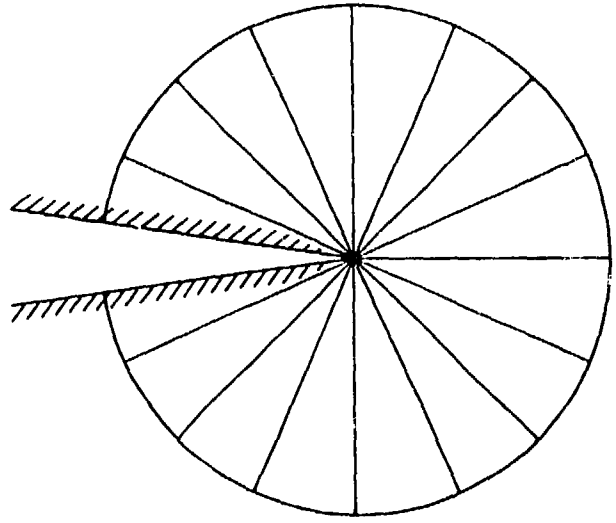

(*a*) ORIGINAL CONFIGURATION

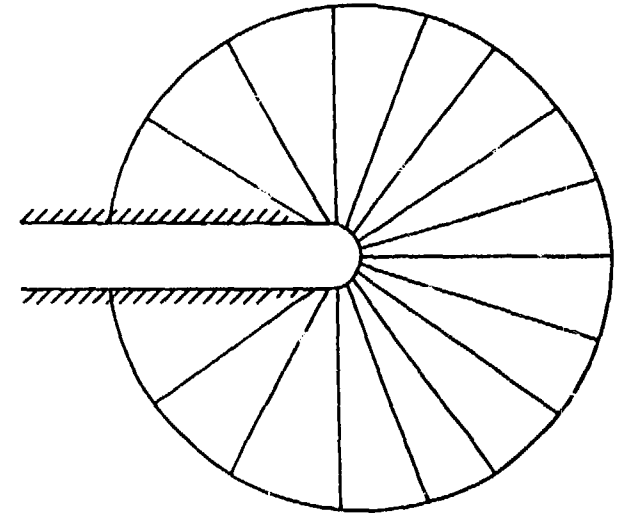

(*b*) DEFORMED CONFIGURATION

FIG. 4

ORNL-DWG 82-8942

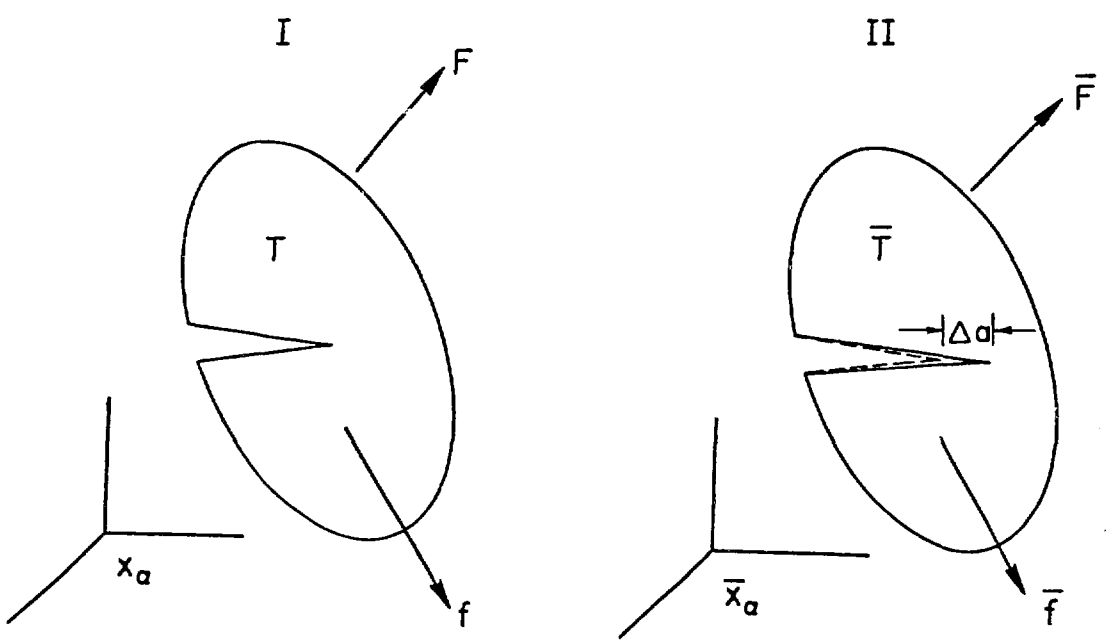

FIG. 5

ORNL-DWG 81-8731A

LOCAL AND UNIFORM ENERGY RELEASE RATES ARE COMPUTED FROM $G=G^*/\Delta A$

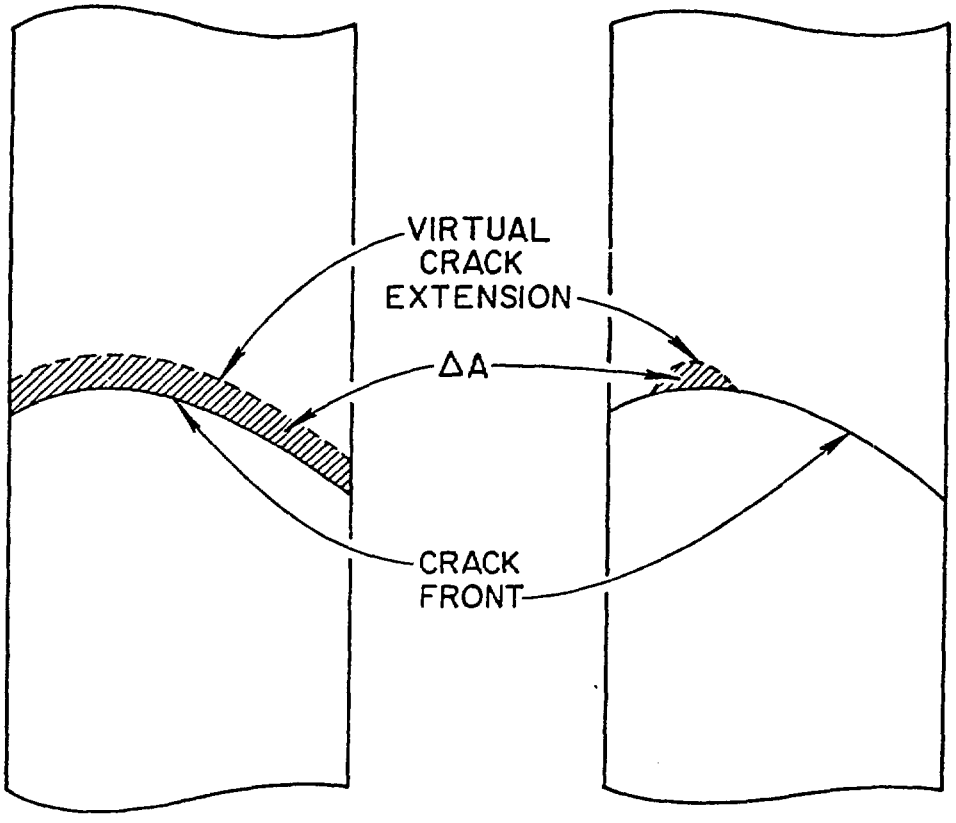

(*a*) UNIFORM EXTENSION (*b*) LOCAL EXTENSION

FIG. 6

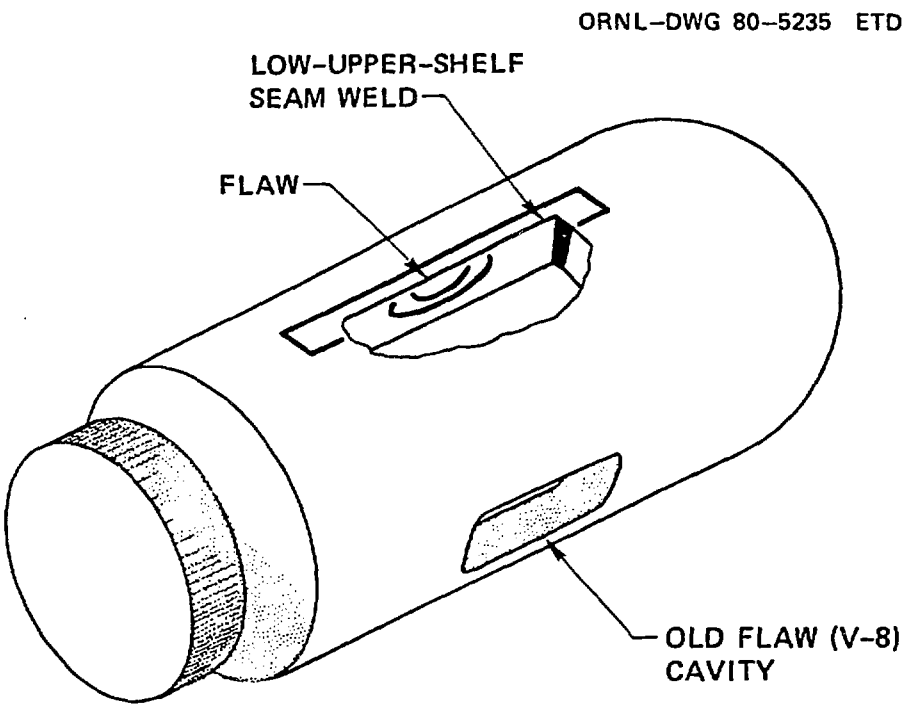
ORNL-DWG 80-5235 ETD
LOW-UPPER-SHELF
SEAM WELD
FLAW
OLD FLAW (V-8)
CAVITY
ITV-8A

FIG. 7

ORNL–DWG 83–4299A ETD

ornl

DESCRIPTION OF ITV V–8A CYLINDER ANALYZED SHOWING CRACK AND QUARTER CYLINDER AS MODELED

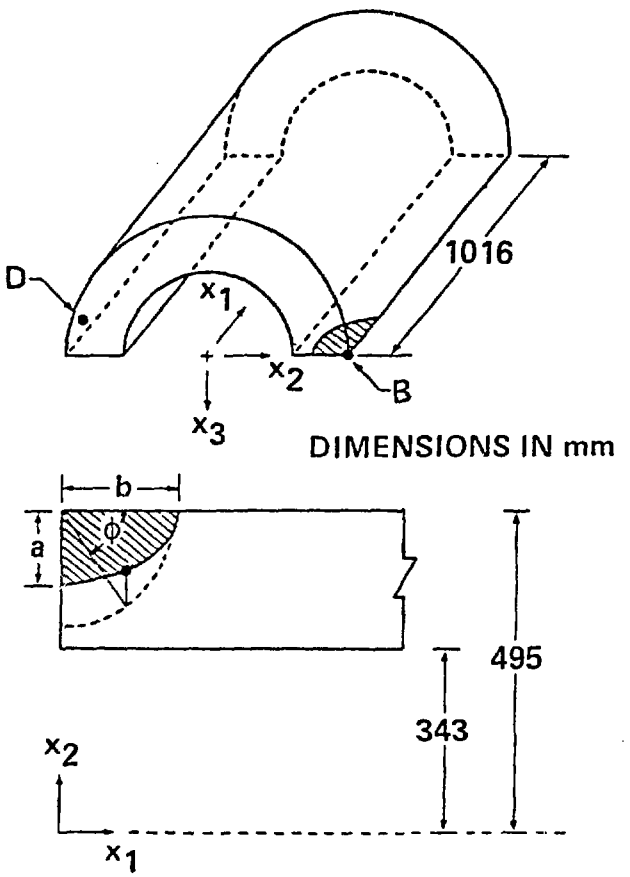

FIG. 8

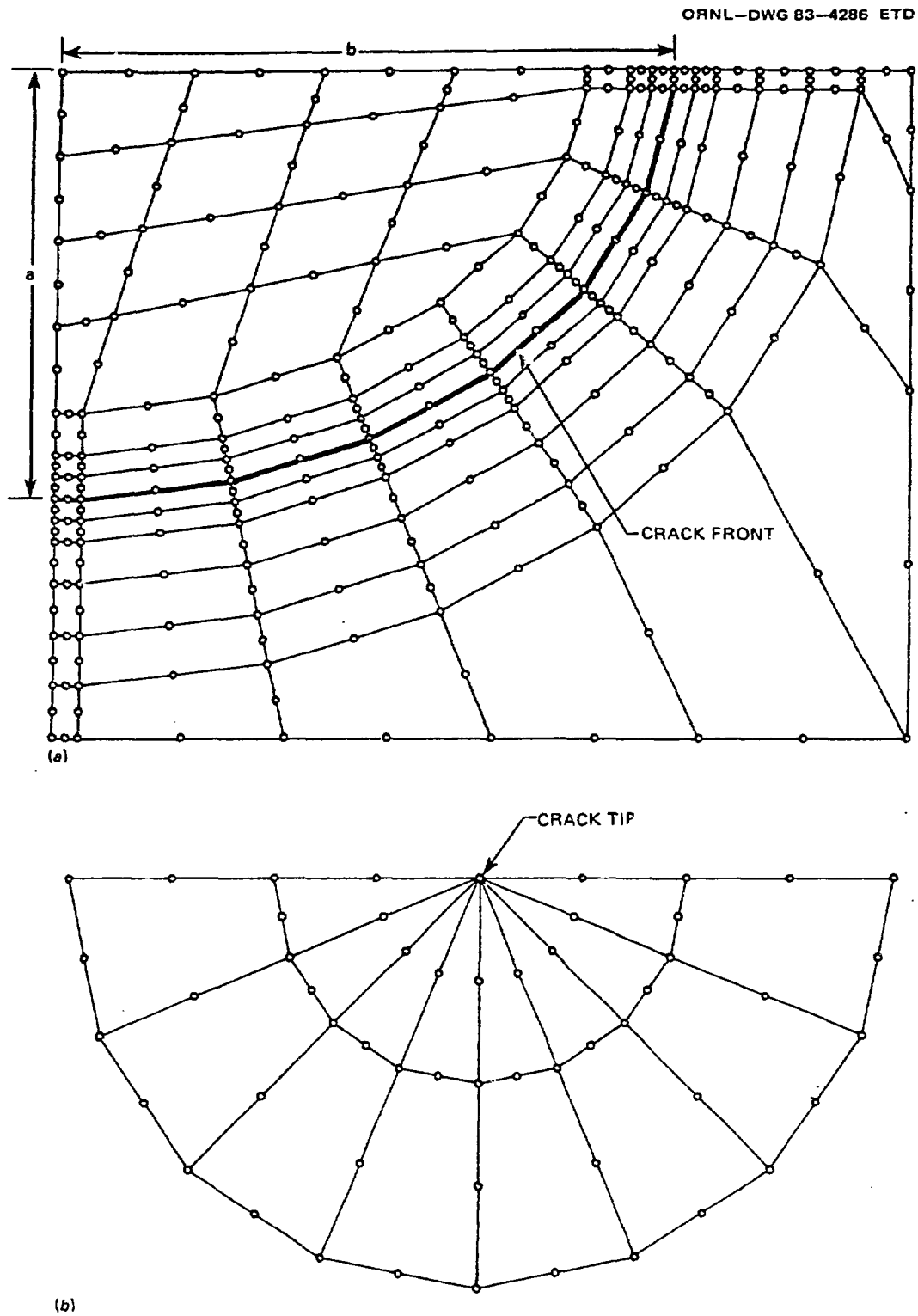

FIG. 9

ORNL–DWG 82–5801A ETD

ornl

UNIAXIAL STRESS–STRAIN CURVE FOR INTERMEDIATE TEST VESSEL V–8A MATERIAL

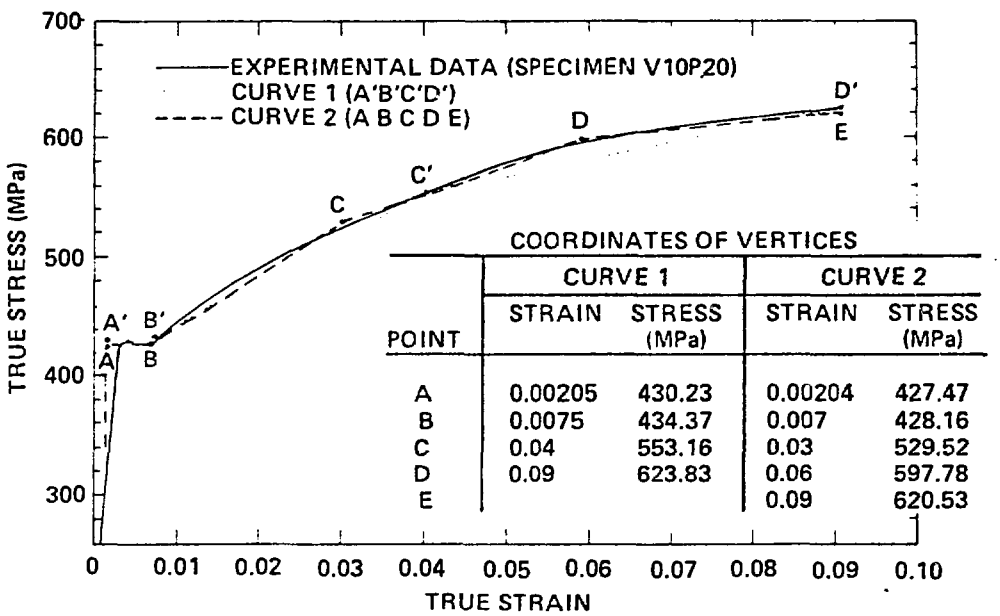

COORDINATES OF VERTICES

POINT	CURVE 1 STRAIN	CURVE 1 STRESS (MPa)	CURVE 2 STRAIN	CURVE 2 STRESS (MPa)
A	0.00205	430.23	0.00204	427.47
B	0.0075	434.37	0.007	428.16
C	0.04	553.16	0.03	529.52
D	0.09	623.83	0.06	597.78
E			0.09	620.53

FIG. 10

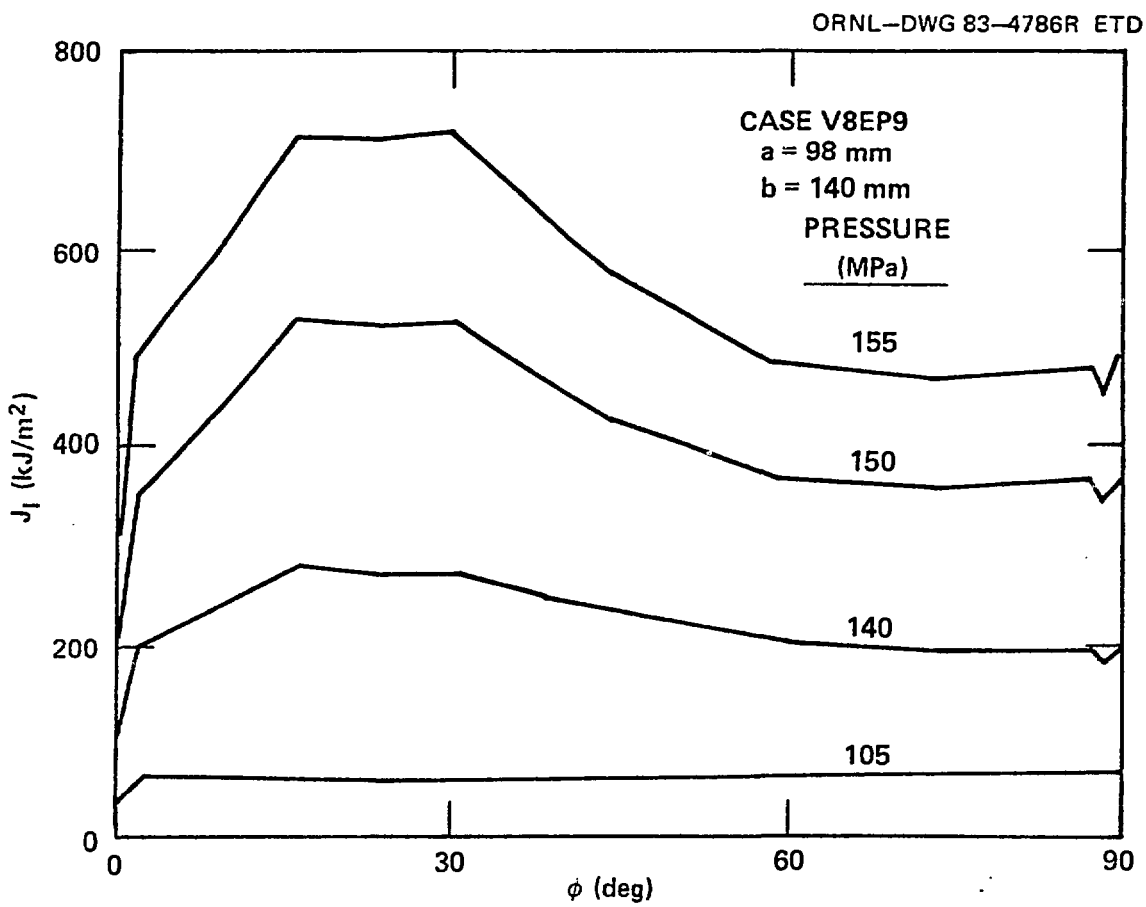
ORNL–DWG 83–4786R ETD
CASE V8EP9
a = 98 mm
b = 140 mm
PRESSURE
(MPa)
155
150
140
105
800
600
400
200
0
0
30
60
90
J_I (kJ/m^2)
ϕ (deg)

FIG. 11

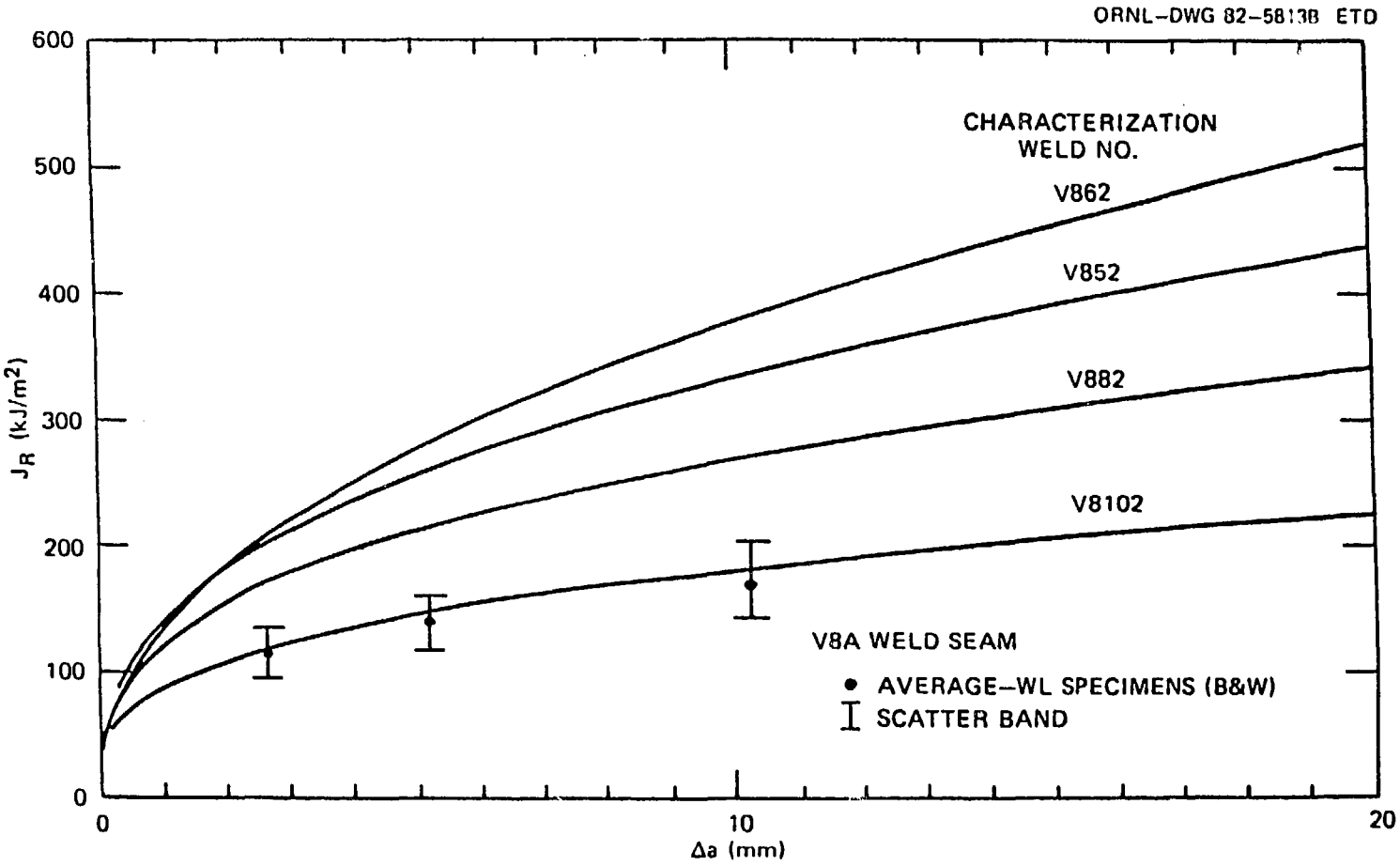
ORNL-DWG 82-58136 ETD
600
500
400
300
200
100
0
J_R (kJ/m^2)
0
10
20
Δa (mm)
CHARACTERIZATION
WELD NO.
V862
V852
V882
V8102
V8A WELD SEAM
AVERAGE-WL SPECIMENS (B&W)
SCATTER BAND

FIG. 12

ORNL–DWG 82–5798 ETD

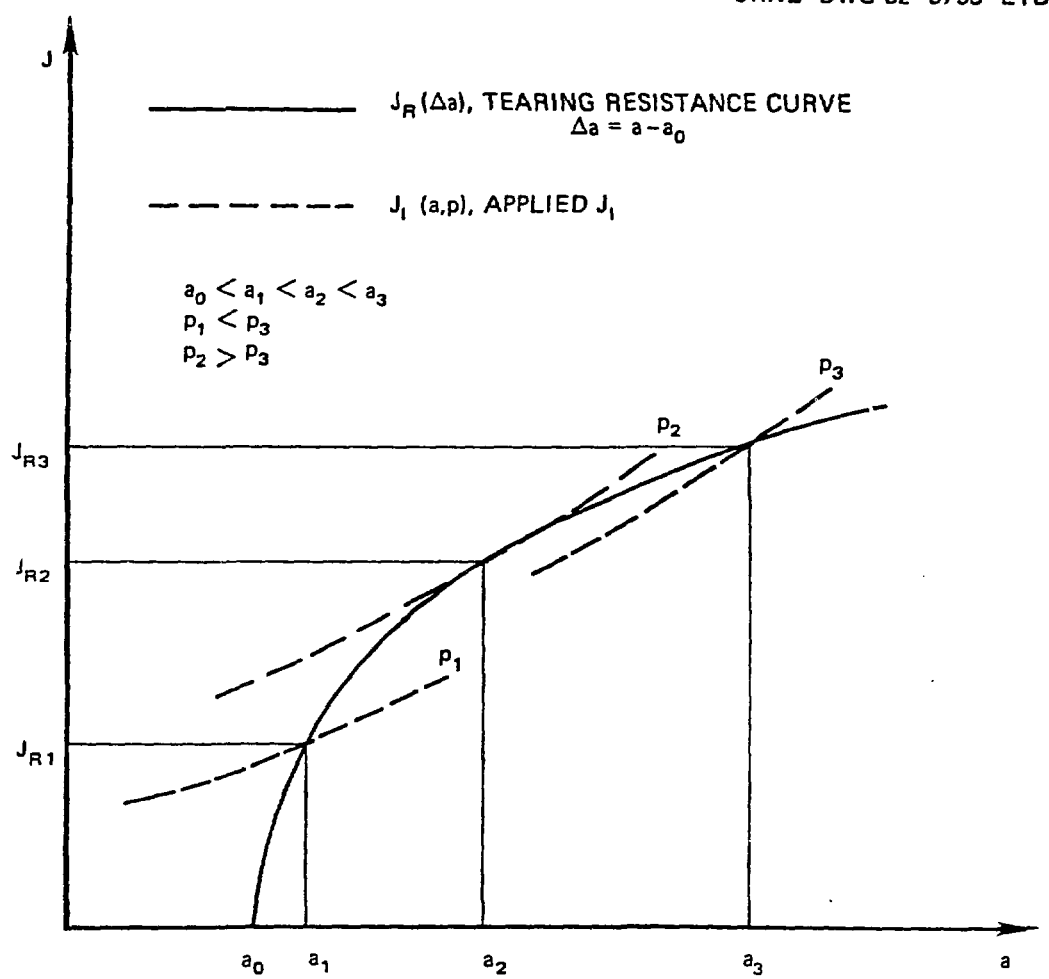

FIG. 13

ORNL PHOTO 6781–83A ETD

ornl

FRACTURE SURFACE (SIDE B) DEVELOPED DURING V–8A TEST. THE DUCTILE FRACTURE SURFACE IS THE RELATIVELY DARK CONTIGUOUS AREA BOUNDED BY THE FATIGUE CRACK EXTENSION AND THE LIGHT–TONE BRITTLE FRACTURE REGIONS GENERATED DURING POSTTEST FRACTURING AT ~ –196°C

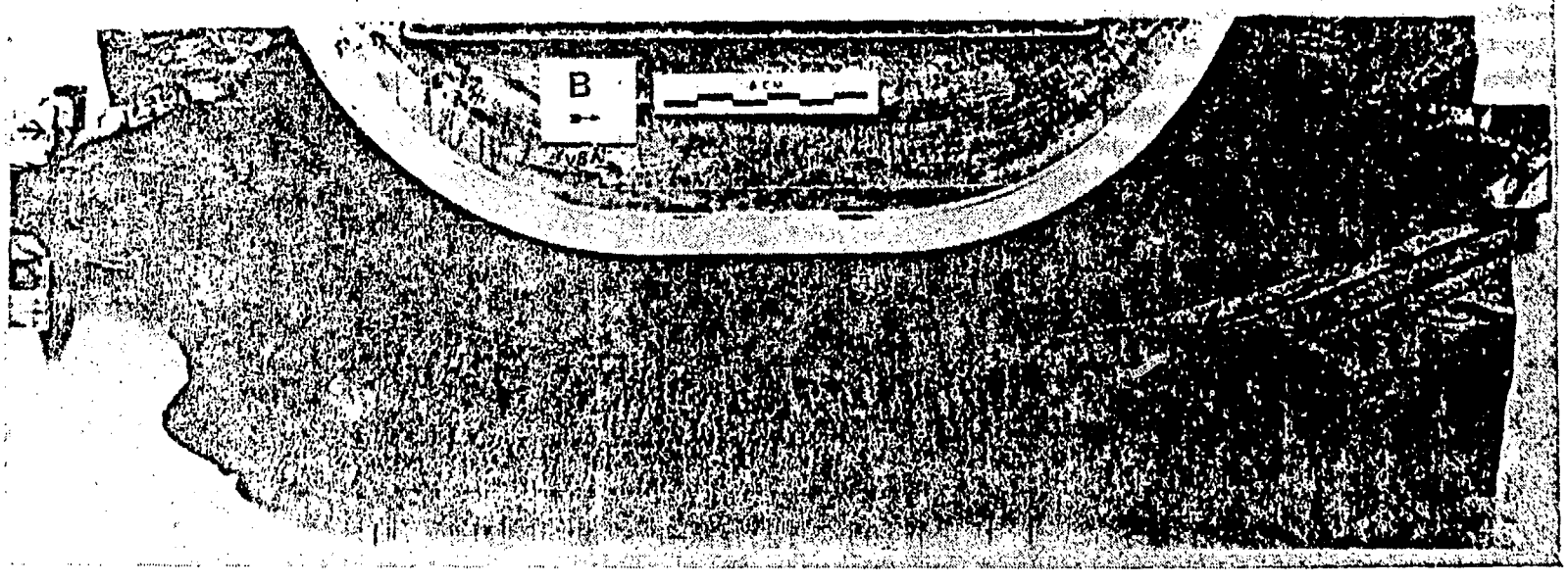

ORNL–DWG 83–5463 ETD

ornl

FOUR CRACK PROFILES SUBJECTED TO POSTTEST ANALYSIS USING ORMGEN/ADINA/ORVIRT

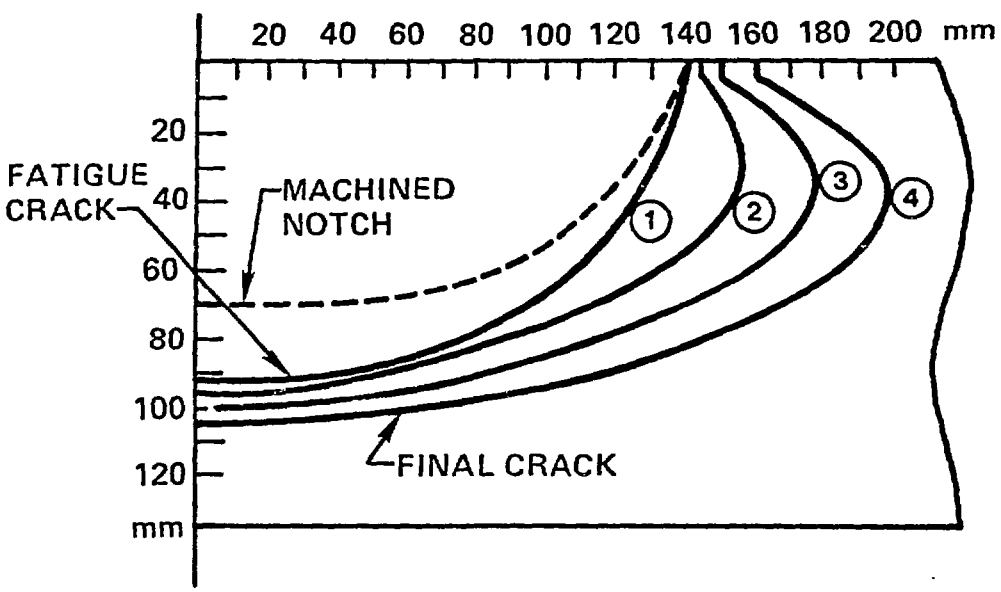

FIG. 15

ORNL–DWG 83–5464 ETD

ornl

FINITE ELEMENT MODEL OF V–8A VESSEL

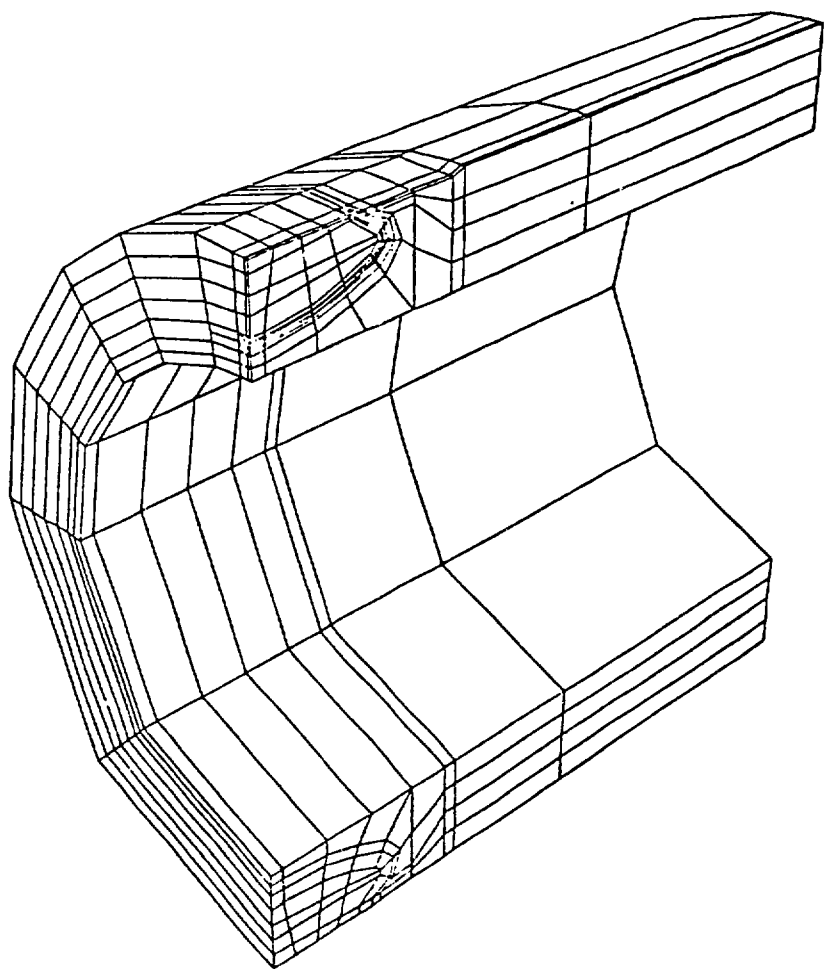

FIG. 16

ORNL–DWG 83–5465 ETD

ornl

J_I VS ϕ AND p FOR INITIAL CRACK PROFILE 1

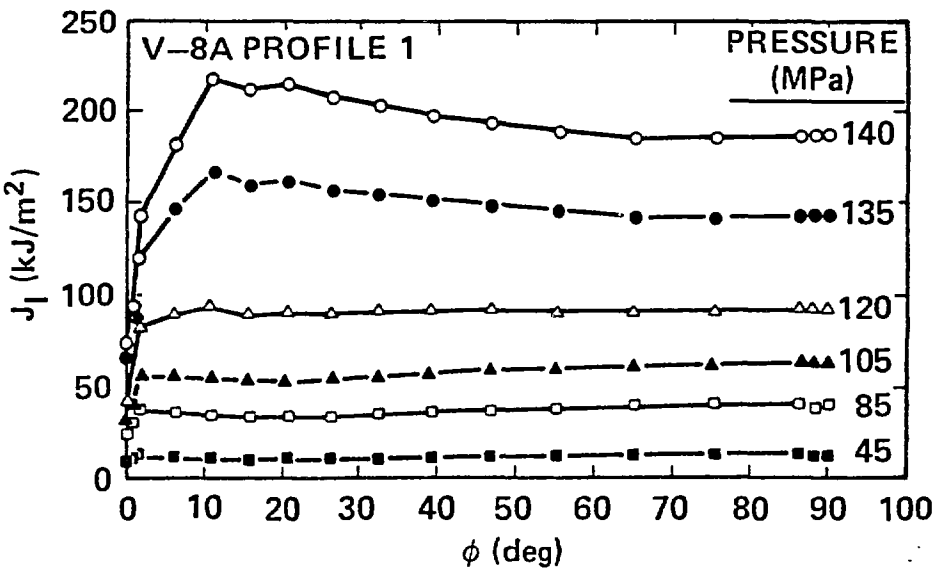

FIG. 17

ORNL–DWG 83–5466 ETD

ornl

J_I VS ϕ AND p FOR INTERMEDIATE CRACK PROFILE 2

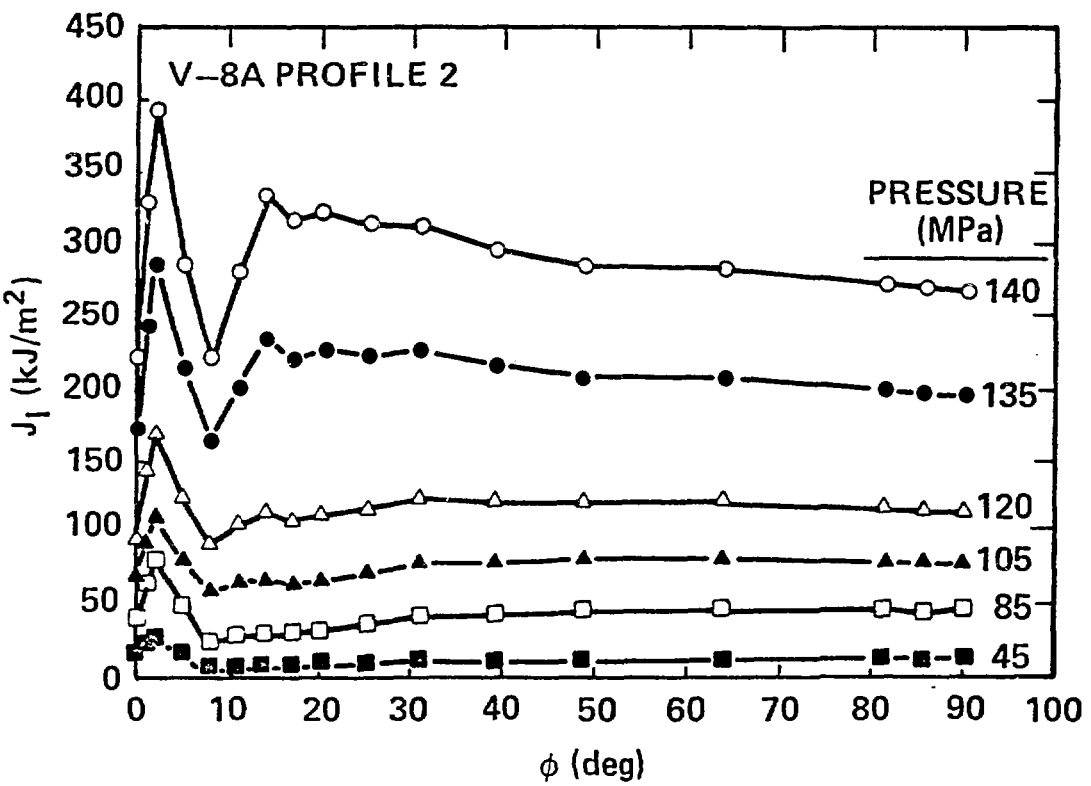

FIG. 18

ORNL–DWG 83–5467 ETD

ornl

J_I VS ϕ AND p FOR INTERMEDIATE CRACK PROFILE 3

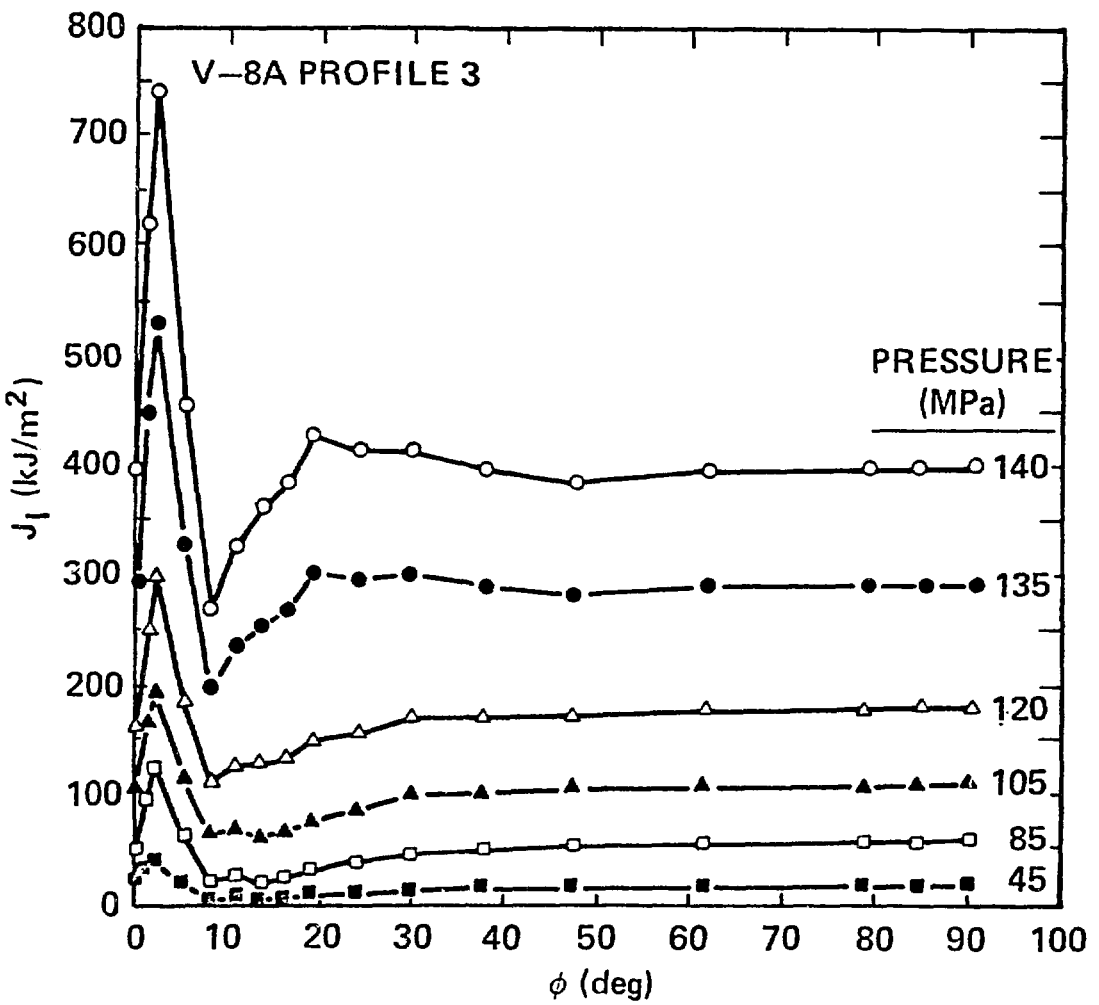

FIG. 19

ORNL–DWG 83–5468 ETD

ornl

J_I VS ϕ AND p FOR FINAL CRACK PROFILE 4

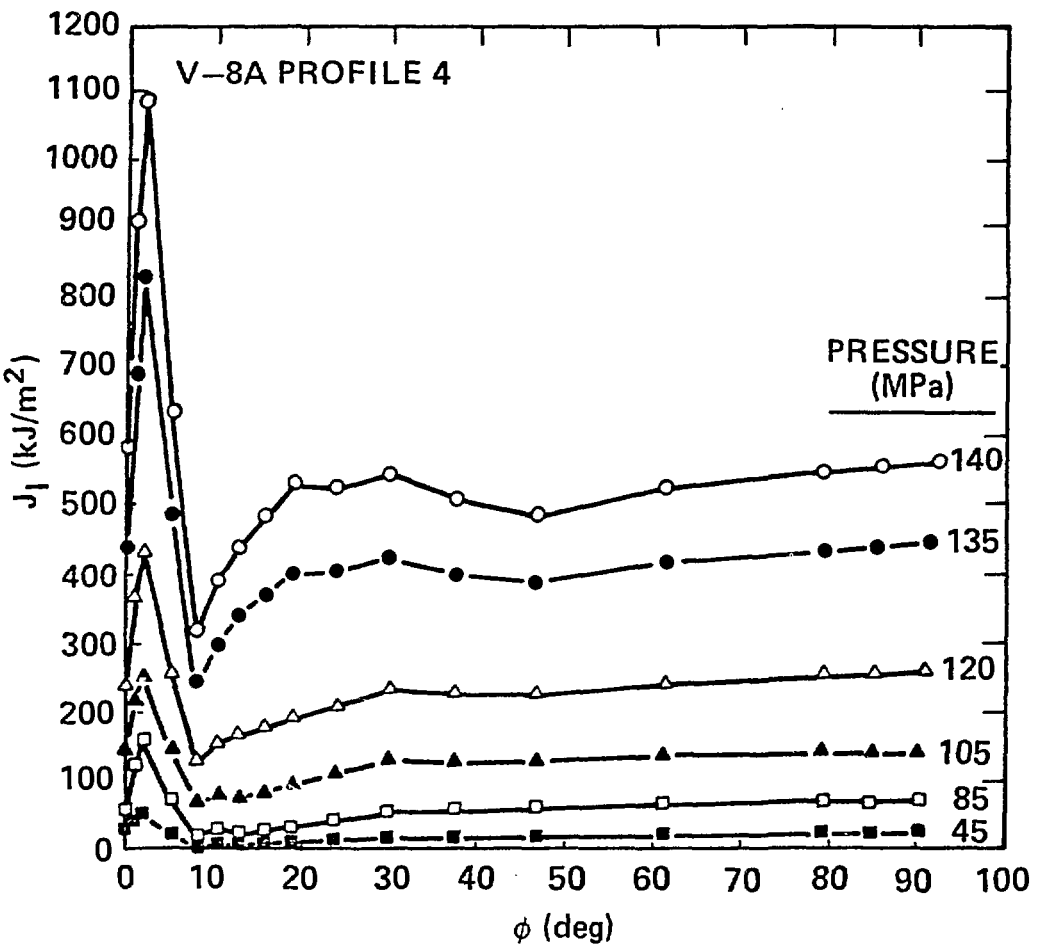

FIG. 20

ORNL–DWG 83–5541 ETD

ornl

J_I VS ϕ AT p = 135 Mpa FOR FOUR CRACK PROFILES

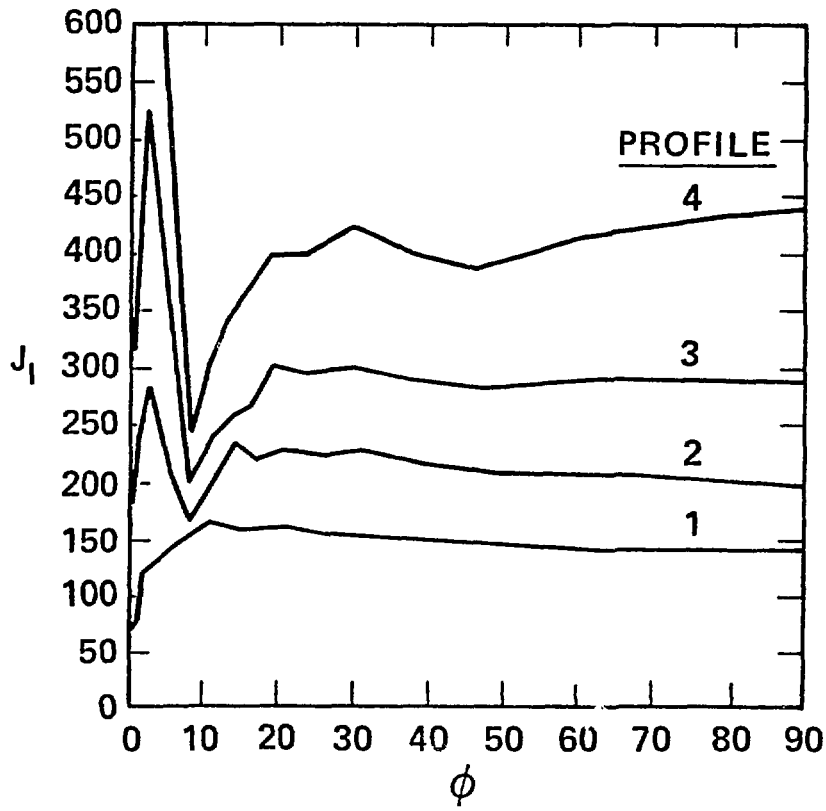

FIG. 21

ORNL–DWG 83–5469 ETD

ornl

A COMPARISON OF MEASURED CMOD WITH COMPUTED CMOD FOR FOUR CRACK PROFILES

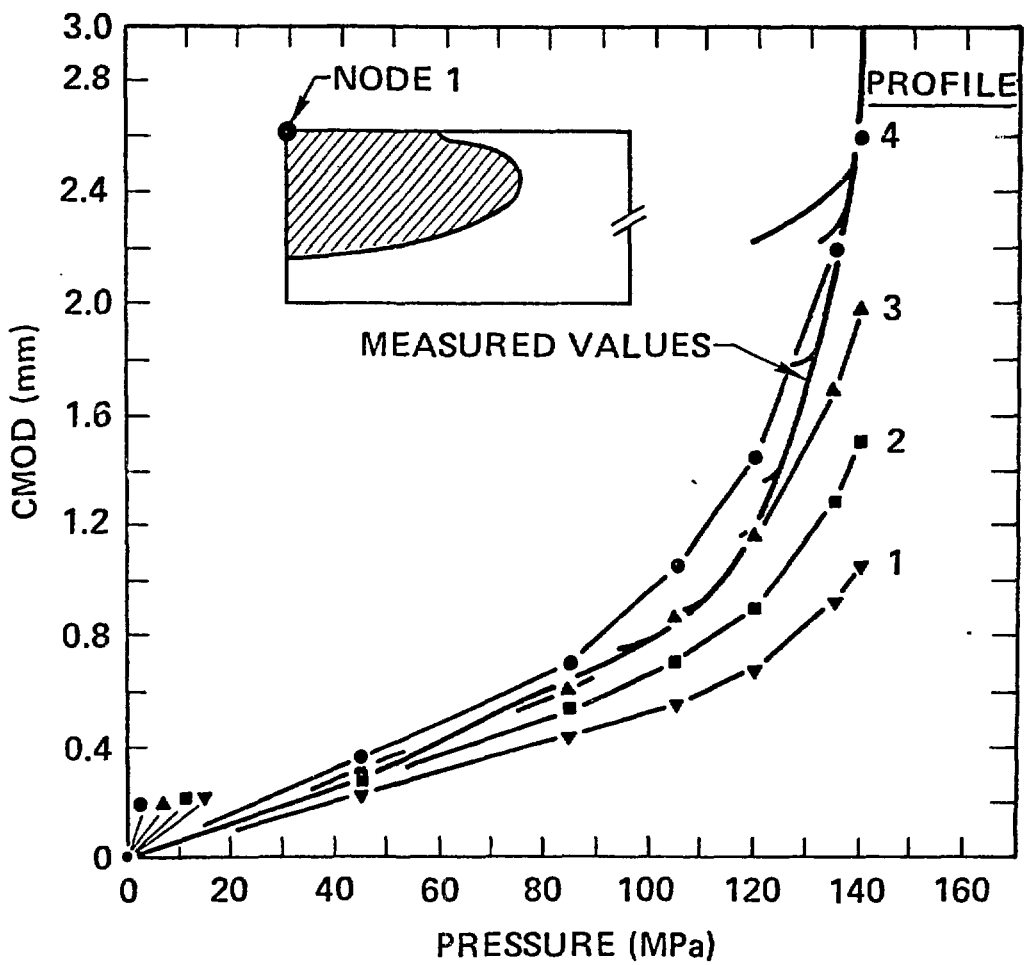

FIG. 22

ORNL–DWG 83–5459 ETD

ornl

PRESSURIZED–THERMAL–SHOCK TEST VESSEL WITH LONGITUDINAL OUTER SURFACE CRACK

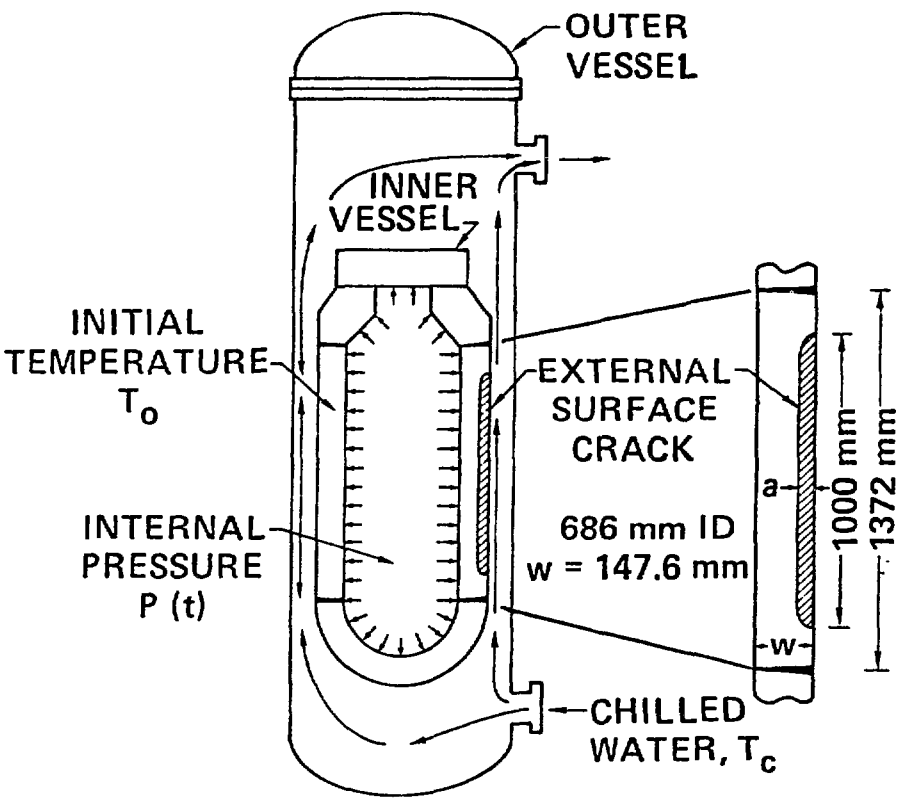

FIG. 23

ORNL–DWG 83–5460 ETD

ornl

SUPERPOSITION PRINCIPLE APPLIED TO A FINITE LENGTH SURFACE CRACK

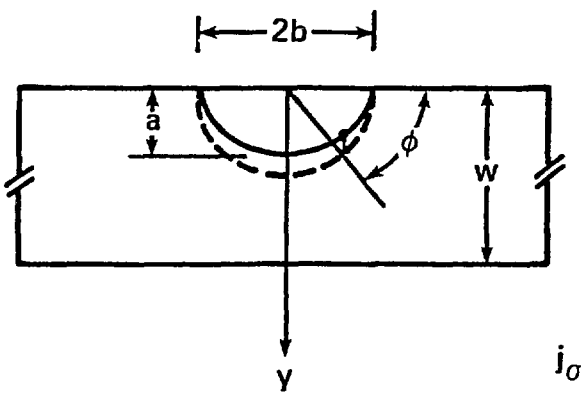

(a)

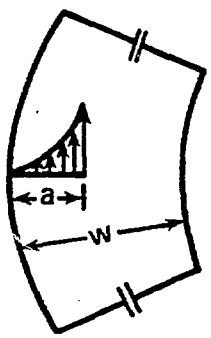

$j_\sigma(y) = (y/a)^j$, j = 0, 1, 2, 3

(b)

FIG. 24

ORNL–DWG 83–4780A ETD

ornl

COMPARISON OF 3–D SUPERPOSITION WITH 3–D DIRECT ANALYSIS FOR FINITE LENGTH SURFACE CRACKS FOR PTS TRANSIENT T1 OF TABLE 4 AT t = 6 min

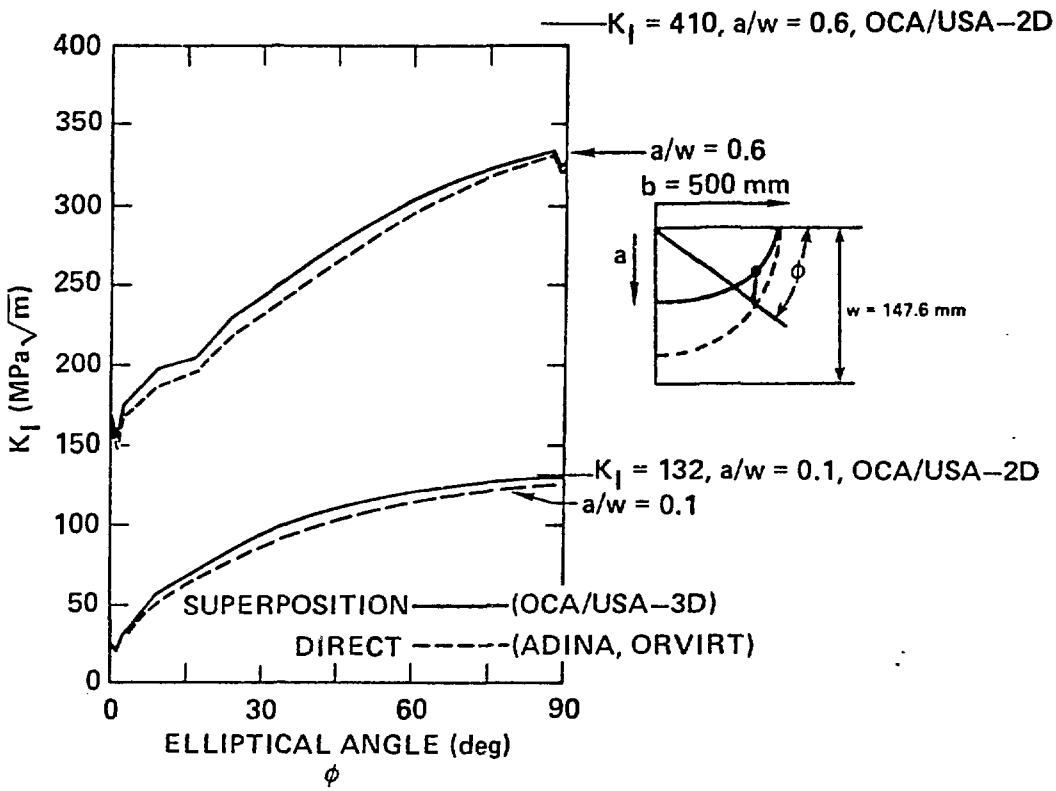

FIG. 25

ORNL–DWG 83–4782 ETD

AN IDEALLY PLASTIC LIGAMENT ANALYSIS IS PERFORMED FOR A DEEP CONTINUOUS EXTERNAL LONGITUDINAL CRACK IN A CYLINDER

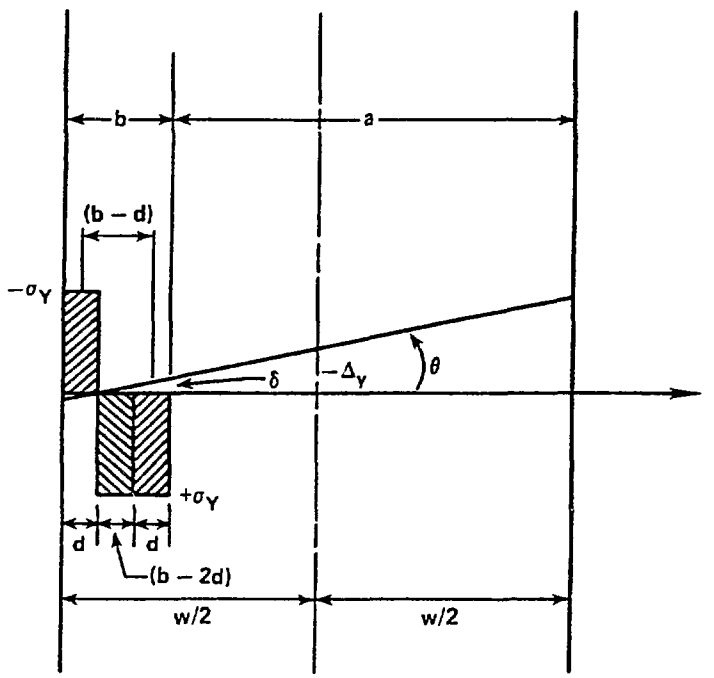

FIG. 26

ORNL–DWG 83–4783A ETD

ornl

COMPARISON OF LIGAMENT ANALYSES FOR PTS TRANSIENT T1 OF TABLE 4 AT t = 6 min

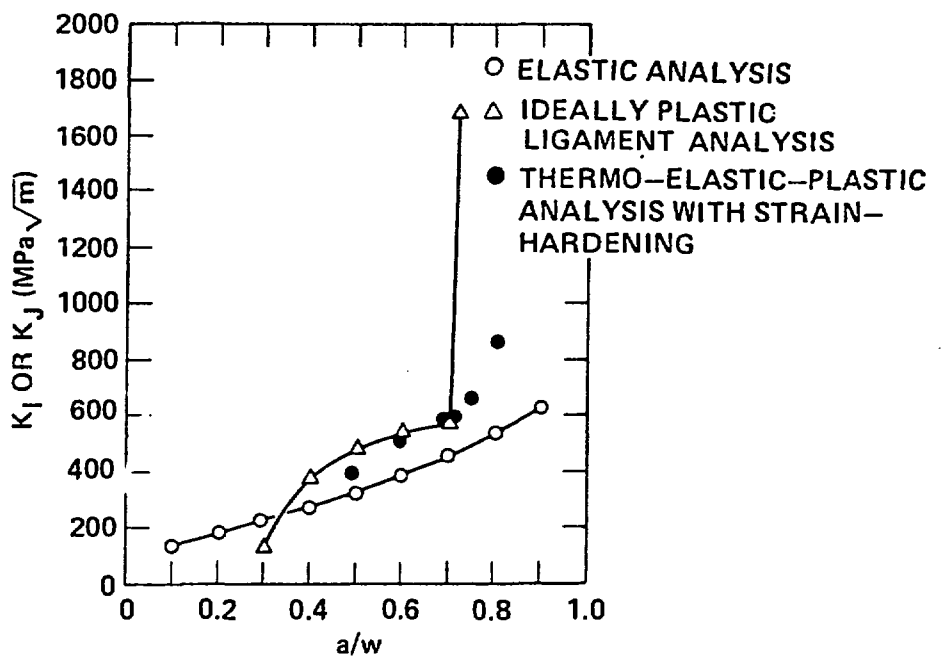

FIG. 27

ORNL–DWG 83–4784A ETD

ornl

UPPER–SHELF ARREST ANALYSIS BASED ON J_R–CONTROLLED TEARING

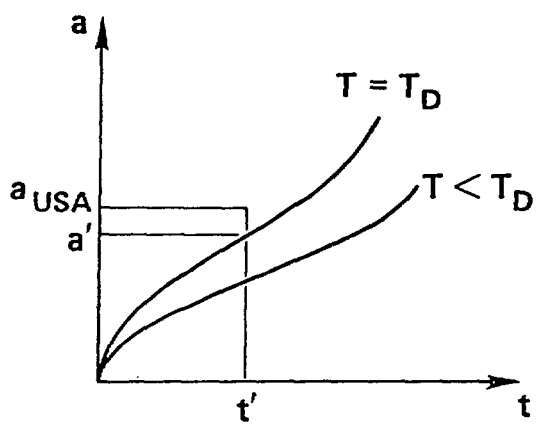

TEMPERATURE CONTOURS

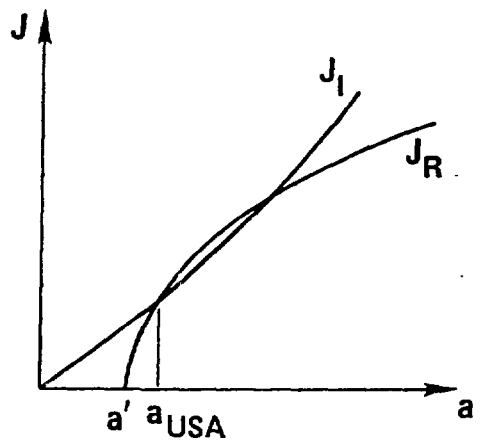

J_I AND J_R AT $t = t'$

FIG. 28

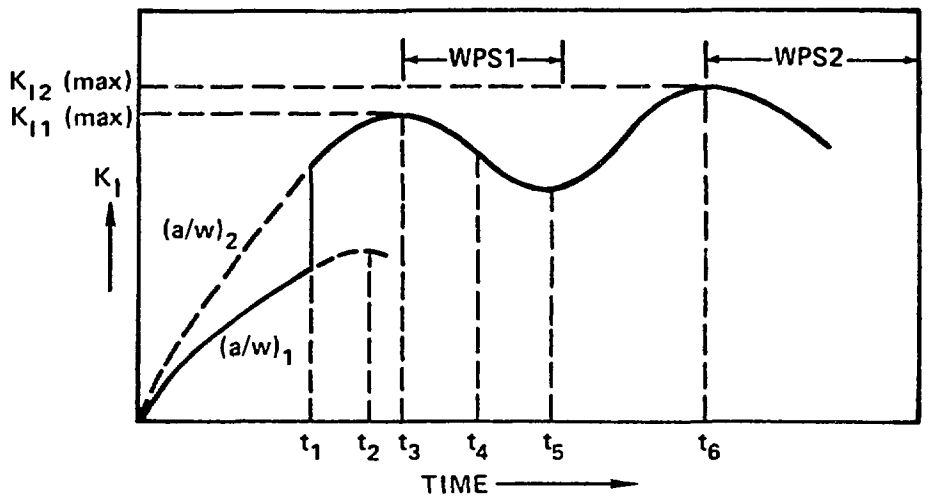

DEFINITIONS:

$(a/w)_1$	= INITIAL CRACK DEPTH
$(a/w)_2$	= CRACK DEPTH AT FIRST ARREST
$(a/w)_{USA}$	= CRACK DEPTH AT UPPER–SHELF ARREST
$(a/w)_{LIG}$	= CRACK DEPTH AT LIGAMENT INSTABILITY
K_{I1} (max)	= K_I AT START OF WPS1
K_{I2} (max)	= K_I AT START OF WPS2
t_{USI}	= TIME OF UPPER–SHELF INSTABILITY

CONDITIONS:

t_1: $K_I/K_{Ic} = 1$ AND INCREASING; $a/w = (a/w)_1$

t_2: $\dot{K}_I = 0$ (K_I max) FOR $a/w = (a/w)_1$; THE START OF WPS FOR $(a/w)_1$

t_3: $\dot{K}_I = 0$ (K_I max) FOR $a/w = (a/w)_2$; THE START OF WPS1

t_4: $K_I/K_{Ic} = 1$ AND INCREASING FOR $a/w = (a/w)_2$

t_5: $\dot{K}_I = 0$ (K_I min) FOR $a/w = (a/w)_2$

t_6: $\dot{K}_I = 0$ (K_I max) FOR $a/w = (a/w)_2$; THE START OF WPS2

CRITERIA:

1. $t_2 - t_1 \geq 30$ s
2. $K_I/K_{Ic} \geq 1.25$ AT t_2, $a/w = (a/w)_1$
3. $K_I/K_{Ic} \geq 1.25$ AT t_5, $a/w = (a/w)_2$
4. K_{I2} (max)$/K_{I1}$ (max) ≥ 1.05, $a/w = (a/w)_2$
5. $\dot{K}_I$ (av) ≤ -6.6 MPa $\cdot\sqrt{m}$/min, $a/w = (a/w)_2$, $t_3 < t < t_5$
6. $T \leq T_{CVN41} + 50^{\circ}C$, $a/w = (a/w)_2$, $t_4 < t < t_6$
7. $T > T_D$ FOR LOCUS OF a/w SATISFYING $K_I = K_{Ia}$, $t_5 < t < t_6$
8. $(a/w)_{USA} < (a/w)_{LIG}$, $t_6 < t_{USI}$

FIG. 29

ORNL–DWG 83–5461 ETD

ornl

CRITICAL CRACK DEPTH AND K_I VS TIME FOR PTS TRANSIENT T2 OF TABLE 1

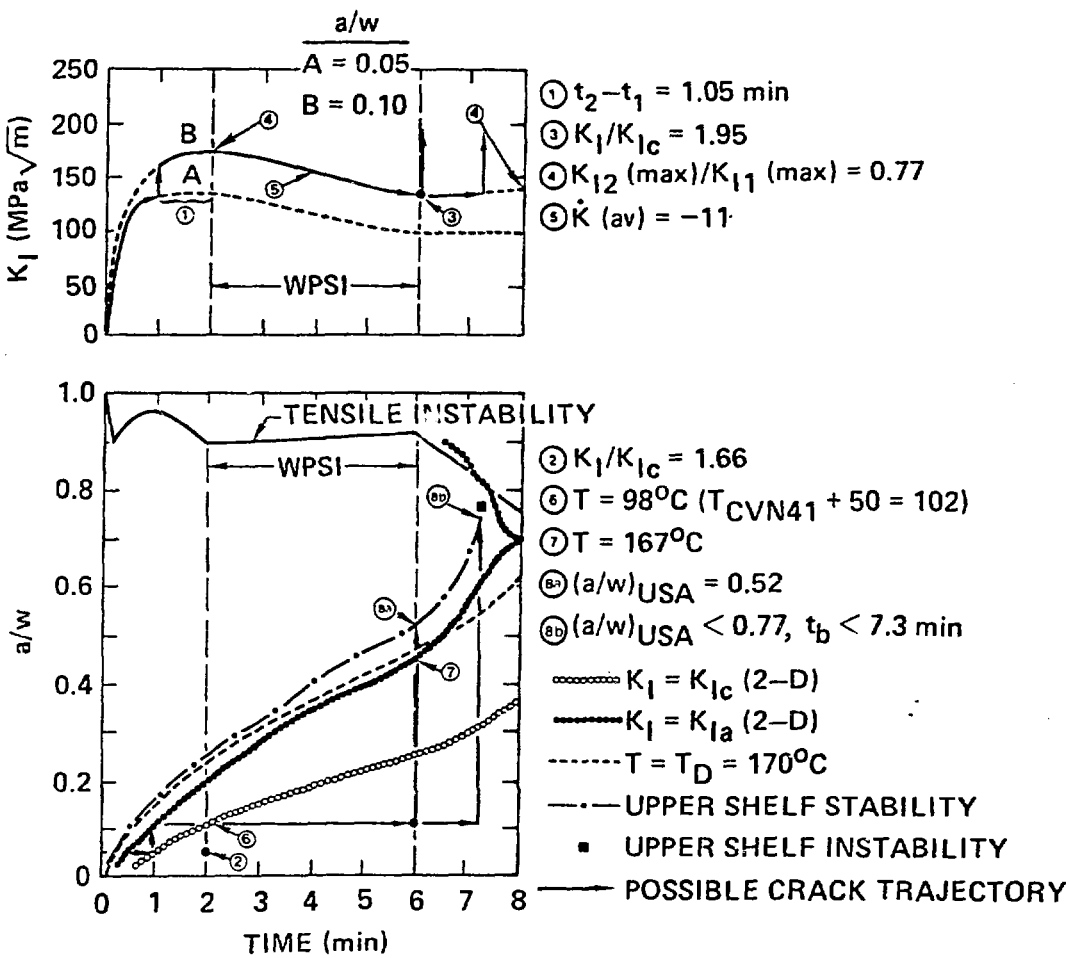

FIG. 30